



JOHN J. HANCOCK  
NAVAL POSTGRADUATE SCHOOL  
MONTEREY, CALIFORNIA 93943-0002





# NAVAL POSTGRADUATE SCHOOL

## Monterey, California



# THESIS

U 145

NUMERICAL SIMULATION OF OPTICAL TURBU-  
LENCE UTILIZING TWO-DIMENSIONAL  
GAUSSIAN PHASE SCREENS

by

Elizabeth Ann Ugorcak

March 1989

Thesis Advisor

Donald L. Walters

Approved for public release; distribution is unlimited.

T242404



classified

Security classification of this page

## REPORT DOCUMENTATION PAGE

Report Security Classification Unclassified		1b Restrictive Markings	
Security Classification Authority		3 Distribution Availability of Report	
Declassification Downgrading Schedule		Approved for public release: distribution is unlimited.	
Performing Organization Report Number(s)		5 Monitoring Organization Report Number(s)	
Name of Performing Organization Naval Postgraduate School	6b Office Symbol (if applicable) 33	7a Name of Monitoring Organization Naval Postgraduate School	
Address (city, state, and ZIP code) Monterey, CA 93943-5000		7b Address (city, state, and ZIP code) Monterey, CA 93943-5000	
Name of Funding Sponsoring Organization	8b Office Symbol (if applicable)	9 Procurement Instrument Identification Number	
Address (city, state, and ZIP code)		10 Source of Funding Numbers	
		Program Element No	Project No
		Task No	Work Unit Accession No

Title (include security classification) NUMERICAL SIMULATION OF OPTICAL TURBULENCE UTILIZING TWO-DIMENSIONAL GAUSSIAN PHASE SCREENS

Personal Author(s) Elizabeth Ann Ugorecak

Type of Report Master's Thesis	13b Time Covered From To	14 Date of Report (year, month, day) March 1989	15 Page Count 70
-----------------------------------	-----------------------------	--	---------------------

Supplementary Notation The views expressed in this thesis are those of the author and do not reflect the official policy or position of the Department of Defense or the U.S. Government.

Cosati Codes			18 Subject Terms (continue on reverse if necessary, and identify by block number) Atmospheric Optical Turbulence, Coherence Length, Mutual Coherence Function, Saturation, Huygens-Fresnel Principle
Id	Group	Subgroup	

Abstract (continue on reverse if necessary and identify by block number)

Propagation of electromagnetic energy through the atmosphere is a difficult task because of temperature fluctuations and index-of-refraction inhomogeneities which degrade the beam's coherence. Understanding this phenomena is of practical importance for optical systems.

This thesis presents an analytical numerical technique which simulates the effects of atmospheric turbulence. The extended Huygens-Fresnel principle was used to simulate wave propagation in a two-dimensional randomly varying medium, which is represented by thin, filtered, Gaussian phase screens. The wave optics code implements both Fresnel and Fraunhofer propagation, by employing the fast Fourier transform (FFT) algorithm. The analytical spatial coherence length,  $\rho_0$ , and normalized intensity variance,  $\sigma^2/I^2$ , of the perturbed electric field, were examined. Results support the concept of intensity saturation for weak scattering cases, however, differences in the values of the theoretical and analytical spatial coherence lengths, occurred.

Distribution Availability of Abstract Unclassified unlimited <input type="checkbox"/> same as report <input type="checkbox"/> DTIC users		21 Abstract Security Classification Unclassified	
Name of Responsible Individual Donald L. Walters		22b Telephone (include Area code) (408) 646-2267	22c Office Symbol 61We

FORM 1473,84 MAR

83 APR edition may be used until exhausted  
All other editions are obsolete

Security classification of this page

Unclassified

Approved for public release; distribution is unlimited.

Numerical Simulation of Optical Turbulence Utilizing Two-Dimensional Gaussian  
Phase Screens

by

Elizabeth Ann Ugorcak  
Lieutenant, United States Navy  
B.S., University of Michigan-Dearborn, 1982

Submitted in partial fulfillment of the  
requirements for the degree of

MASTER OF SCIENCE IN PHYSICS

from the

NAVAL POSTGRADUATE SCHOOL  
March 1989

## ABSTRACT

Propagation of electromagnetic energy through the atmosphere is a difficult task because of temperature fluctuations and index-of-refraction inhomogeneities which degrade the beam's coherence. Understanding this phenomena is of practical importance for optical systems.

This thesis presents an analytical/numerical technique which simulates the effects of atmospheric turbulence. The extended Huygens-Fresnel principle was used to simulate wave propagation in a two-dimensional randomly varying medium, which is represented by thin, filtered, Gaussian phase screens. The wave optics code implements both Fresnel and Fraunhofer propagation, by employing the fast Fourier transform (FFT) algorithm. The analytical spatial coherence length,  $\rho_0$ , and normalized intensity variance,  $\sigma^2/I^2$ , of the perturbed electric field, were examined. Results support the concept of intensity saturation for weak scattering cases, however, differences in the values of the theoretical and analytical spatial coherence lengths, occurred.

1/10/20  
1995  
C.1

## TABLE OF CONTENTS

I. INTRODUCTION .....	1
II. BACKGROUND .....	2
A. STATISTICAL DESCRIPTION OF TURBULENCE .....	2
1. Random Variables .....	2
2. Local Homogeneity and Isotropy .....	2
3. Structure Functions .....	2
4. Covariance, Power Spectral Densities .....	3
B. EM PROPAGATION THROUGH TURBULENCE .....	5
1. Wave Equation .....	5
2. The Method of Small Perturbations-Born Approximation .....	6
3. The Method of Smooth Perturbations-Rytov Approximation .....	7
C. HUYGENS-FRESNEL THEORY .....	7
D. MUTUAL COHERENCE FUNCTION .....	8
E. MODULATION TRANSFER FUNCTION .....	9
F. DIFFRACTION INTEGRAL .....	10
III. NUMERICAL SIMULATION MODEL .....	15
A. EXPERIMENTAL ARRANGEMENT .....	15
B. COMPUTER PRELIMINARIES .....	15
1. Random number generator .....	15
2. Fast Fourier Transform .....	16
C. PROCEDURE .....	18
1. Input Parameters .....	18
2. Aperture Mutual Coherence Function .....	18
3. Planar Electric Field .....	18
4. Phase Screens .....	21
a. Generation .....	21
b. Filtering .....	21
5. Implementation .....	22
6. Propagation Methods .....	23

a. Fraunhofer .....	23
b. Fresnel .....	23
7. Atmospheric Mutual Coherence Function .....	27
IV. RESULTS .....	28
A. FILTERING .....	28
B. MCF .....	29
C. SATURATION .....	38
V. CONCLUSIONS AND RECOMMENDATIONS .....	40
APPENDIX A. RANDOM NUMBER GENERATOR TEST DATA .....	41
APPENDIX B. FFT TIME SERIES DATA .....	42
APPENDIX C. SIMULATION CODE .....	43
LIST OF REFERENCES .....	59
INITIAL DISTRIBUTION LIST .....	61

## LIST OF FIGURES

Figure 1.	Short Term Mutual Coherence Function for an 8 x 8 Subaperture. . . . .	11
Figure 2.	Conceptual Diagram of the Simulation Coding. . . . .	19
Figure 3.	Three Dimensional Perspective of the Initial Electric Field. . . . .	20
Figure 4.	Three Dimensional Diffraction Pattern for an 8 x 8 Subaperture. . . . .	24
Figure 5.	Three Dimensional Diffraction Pattern of a 16 x 16 Subaperture. . . . .	25
Figure 6.	Perturbed Diffraction Pattern of a 16 x 16 Subaperture. . . . .	26
Figure 7.	Filtered Phase Screen of a 16 x 16 Subaperture. . . . .	30
Figure 8.	Filtered Phase Screen of a 32 x 32 Subaperture. . . . .	31
Figure 9.	Filtered Phase Screen of a 64 x 64 Subaperture. . . . .	32
Figure 10.	Computed Autocorrelation of a Square Subaperture. . . . .	33
Figure 11.	Mutual Coherence Function of a 64 x 64 Subaperture. . . . .	34
Figure 12.	Mutual Coherence Function Trends. . . . .	35
Figure 13.	Subaperture Coherence Lengths for $C_n^2 = 1 \times 10^{-13}$ . . . . .	36
Figure 14.	Subaperture Coherence Lengths for $C_n^2 = 1 \times 10^{-14}$ . . . . .	37
Figure 15.	Intensity Variance Saturation of a 16 x 16 Subaperture. . . . .	39

## ACKNOWLEDGEMENTS

My deepest appreciation to Dr. Walters for providing the knowledge and experience necessary for the successful completion of this thesis. His enthusiasm and sincerity were invaluable to me during my tour at NPS. I would also like to thank Gail Tirrell Vaucher and Chris Vaucher for their moral support, assistance, and especially, their friendship. Finally, thank you Phyllis.



# I. INTRODUCTION

Atmospheric turbulence degrades the coherence of electromagnetic energy propagating through the atmosphere. The refractive-index inhomogeneities associated with the turbulent atmosphere induce phase and intensity perturbations across the wavefront. Understanding the propagation and scattering of optical waves in random media, is essential for atmospheric laser beam propagation and imaging systems.

This thesis models the propagation through a random media by means of the extended Huygens-Fresnel principle. A two-dimensional, thin, Gaussian phase screen represents the randomly varying medium. This wave optics propagation code employs the fast Fourier transform (FFT) algorithm in both Fresnel and Fraunhofer forms of propagation. The Fresnel region incorporates two forms of the diffraction integral, the transfer function form for "near field" distances, and the convolution form for "far field" regions.

Previously, numerically intensive simulations of this type required large, super-computer systems. However, these computations were performed on a compact, desktop computer system.

The model's accuracy was assessed by comparing computer values of the spatial coherence length,  $\rho_0$ , with values obtained from the analytical mutual coherence function (MCF). Additionally, the concept of intensity variance saturation was examined for a single phase screen in the Fraunhofer approximation. The normalized intensity variance,  $\sigma_I^2/I$ , approaches a saturation value asymptotically for increasing values of the index-of-refraction structure parameter,  $C_n^2$ . Theoretical calculations suggest saturation for multiple scattering, however, they say nothing about a single phase screen realization. This thesis provides results which support saturation effects for single scattering cases.

## II. BACKGROUND

### A. STATISTICAL DESCRIPTION OF TURBULENCE

#### 1. Random Variables

Maintaining the coherence of an electromagnetic wave propagating through the atmosphere, requires an understanding of the effects imposed on the wave by the turbulent medium. The fundamental characteristic of atmospheric turbulence is its randomness, which must be described statistically. In addition to statistical quantities, further assumptions must be made of atmospheric turbulence. These include the concepts of stationarity, homogeneity and isotropy. Stationarity implies that random processes are time independent. Homogeneity assumes invariance under a Galilean transformation of coordinates, while isotropic variables are invariant with respect to coordinate rotations. [Ref. 1] Mathematically, these two assumptions imply that the statistics at two points  $\vec{r}_1$  and  $\vec{r}_2$  depend only on the difference,  $r_{12} = |\vec{r}_1 - \vec{r}_2|$ .

#### 2. Local Homogeneity and Isotropy

In general, atmospheric random variables do not obey the assumptions of stationarity, homogeneity, and isotropy. However, Tatarski [Ref. 2] introduces the concept of "local" homogeneous and isotropic random variables. This concept requires homogeneity and isotropy within a localized region of size  $L_0$ , the outer scale length. Furthermore, the difficulties associated with nonstationary random variables, are removed by considering random fields with stationary first increments [Ref. 2]. Tatarski's method applies to a nonstationary random function whose mean varies slowly with time, by considering the difference of the function at two different locations. The slow functional changes do not affect the value of this difference.

#### 3. Structure Functions

Tatarski introduces the structure function

$$D_f(\vec{r}_2 - \vec{r}_1) = \langle [f(\vec{r}_2) - f(\vec{r}_1)]^2 \rangle, \quad (1)$$

a tensor that is the difference between two quantities. Some important aspects of the structure function are; that its general form is valid for any variable, and  $\langle \rangle$  denotes an ensemble average taken over all possible point pairs  $\vec{r}_2, \vec{r}_1$ . Assuming homogeneity and isotropy, the vector dependence reduces to the magnitude  $r_{12} = |\vec{r}_2 - \vec{r}_1|$ , and the structure function becomes

$$D_f(r) = \langle [f(r_2) - f(r_1)]^2 \rangle. \quad (2)$$

Kolmogorov showed through dimensional analysis, a simple power law dependence of equation (2), over a limited interval called the inertial subrange, as

$$D_f(r) = C_f^2 r^{2/3}. \quad (3)$$

Tatarski introduces the concept of "passive additives", which are quantities independent of position in the vector field, and do not directly influence the dynamics of the turbulent medium. Temperature is a passive additive and has a structure function of the form

$$D_T(r) = C_T^2 r^{2/3}. \quad (4)$$

As long as  $r$  remains within the inertial subrange, temperature is approximated as a passive additive, and equation (4) is valid. Likewise the index-of-refraction is a passive additive with a structure function

$$D_n(r) = C_n^2 r^{2/3}. \quad (5)$$

Since the index of refraction depends on the density of the atmosphere,  $D_n$  and  $D_T$  are related by

$$D_n = D_T \left( 79 \times 10^{-6} \frac{P}{T^2} \right)^2. \quad (6)$$

#### 4. Covariance, Power Spectral Densities

In addition to the structure function, other characteristics of random processes include the covariance (or correlation), and Power Spectral Densities. It is the interrelationship of these three quantities which provide a useful method for analyzing random processes. The covariance between two random variables  $S$  and  $T$  can be expressed as

$$B_{ST} = \langle [T(r_1) - \langle T(r_1) \rangle] [S(r_2) - \langle S(r_2) \rangle] \rangle. \quad (7)$$

However, more frequently it is the autocovariance function

$$B_{TT} = \langle [T(r_1) - \langle T(r_1) \rangle] [T(r_2) - \langle T(r_2) \rangle] \rangle, \quad (8)$$

which is needed. Furthermore, if  $T$  is homogeneous and  $\langle T \rangle = 0$  is assumed, then equation (8) simplifies to

$$B_T(r) = \langle T(r_1)T(r_2) \rangle. \quad (9)$$

Combining this relation and equation (2), gives an expression for the relationship between the structure function and covariance function as

$$D_T(r) = 2[B_{TT}(0) - B_{TT}(r)]. \quad (10)$$

In one dimension the covariance function and the power spectral density are transform pairs given by

$$W(\kappa) = \int_{-\infty}^{+\infty} e^{-i\kappa r} B(r) dr, \quad (11)$$

and

$$B(r) = \frac{1}{2\pi} \int_{-\infty}^{+\infty} e^{i\kappa r} W(\kappa) d\kappa. \quad (12)$$

Using the fact that  $B(r)$  is an even function and substituting equation (12) into equation (10),  $D(r)$  becomes,

$$D(r) = 2 \int_{-\infty}^{+\infty} [1 - \cos(\kappa r)] W(\kappa) d\kappa. \quad (13)$$

Tatarski develops an expression for the one-dimensional Kolmogorov spectral density, given by

$$W(\kappa) = 0.1224 C_n^2 \kappa^{-5/3}. \quad (14)$$

Discussion to this point has been of one-dimensional random processes, however these concepts are applicable to three-dimensional cases. Analogous to equation (11), Tatarski defines the three-dimensional power spectral density as

$$\Phi(\bar{\kappa}) = \int_{-\infty}^{+\infty} \int_{-\infty}^{+\infty} \int_{-\infty}^{+\infty} e^{-i\bar{\kappa} \cdot \bar{r}} B(\bar{r}) d^3 \bar{r}, \quad (15)$$

and similarly, the correlation function is

$$B(\bar{r}) = \frac{1}{(2\pi)^3} \int_{-\infty}^{+\infty} \int_{-\infty}^{+\infty} \int_{-\infty}^{+\infty} e^{i\bar{\kappa} \cdot \bar{r}} \Phi(\bar{\kappa}) d^3 \bar{\kappa}. \quad (16)$$

Using the relation

$$\Phi(\kappa) = \frac{-1}{2\pi\kappa} \frac{dW(\kappa)}{d\kappa}, \quad (17)$$

the three-dimensional Kolmogorov power spectral density becomes

$$\Phi(\kappa) = 0.033 C_n^2 \kappa^{-11/3}. \quad (18)$$

## B. EM PROPAGATION THROUGH TURBULENCE

### 1. Wave Equation

Based upon Tatarski, Clifford [Ref. 3] develops theoretical results of line-of-sight propagation through the atmosphere, directly from Maxwell's equations. Assuming zero conductivity, and unit magnetic permeability in the atmosphere, as well as, a sinusoidal time dependent electromagnetic field, Maxwell's four equations, in Gaussian units, take the form

$$\nabla \cdot \bar{H} = 0, \quad (19)$$

$$\nabla \times \bar{E} = ik\bar{H}, \quad (20)$$

$$\nabla \times \bar{H} = -ikn^2 \bar{E}, \quad (21)$$

$$\nabla \cdot (n^2 \bar{E}) = 0. \quad (22)$$

Taking the curl of equation (20), and substituting it into equation (21), gives

$$-\nabla^2 \bar{E} + \nabla(\nabla \cdot \bar{E}) = k^2 n^2 \bar{E}. \quad (23)$$

Rewriting equation (22) in the form

$$\bar{E} \cdot \nabla n^2 + n^2 \nabla \cdot \bar{E} = 0, \quad (24)$$

and substituting it into equation (23), yields the vector form of the wave equation

$$\nabla^2 \bar{E} + k^2 n^2 \bar{E} + 2\nabla(\bar{E} \cdot \nabla \log n) = 0. \quad (25)$$

The third term of equation (25) describes the change in polarization of a propagating electromagnetic wave. This term is negligible as long as the wavelength is small compared to the refractive inhomogeneities. Thus equation (25) reduces to

$$\nabla^2 \bar{E} + k^2 n^2 \bar{E} = 0. \quad (26)$$

Equation (26) is the vector form of the wave equation describing propagation through the turbulent atmosphere. The difficulty in solving this equation lies in the second term containing the random variable  $n$ . Various methods are available for obtaining solutions to equation (26), each of which relies on several critical approximations. Strohbehn [Ref. 4] lists these approximations as:

1. Negligible depolarization effects.
2. Negligible back-scattering.
3. Use of the parabolic approximation to the wave equation.
4. Turbulence is uncorrelated in the direction of propagation.

## 2. The Method of Small Perturbations-Born Approximation

Both Tatarski [Ref. 2] and Clifford [Ref. 3], solve the wave equation in a turbulent atmosphere using the method of small perturbations, which is equivalent to the Born approximation. This method expands the electric field into a series of decreasing amplitudes, and the refractive index into a power series in the form

$$E = E_0 + E_1 + \dots \quad (27)$$

$$n = 1 + n_1 + \dots \quad (28)$$

Substituting these into equation (26) and equating same order terms, results in two equations

$$\nabla^2 E_0 + k^2 E_0 = 0, \quad (29)$$

$$\nabla^2 E_1 + k^2 E_1 + 2k^2 n_1 E_0 = 0, \quad (30)$$

where terms of order  $n_1^2$  and higher are ignored. Assuming, as Tatarski does, that the unperturbed field is a plane wave propagating in the  $z$ -direction represented as  $E_0 = \exp[ikz]$ , equation (30) becomes

$$\nabla^2 E_1 + k^2 E_1 = -2k^2 n_1 e^{ikz}, \quad (31)$$

an inhomogeneous partial differential equation with constant coefficients. Its solution is the convolution of a plane wave Green's function with the source term, or inhomogeneous term, given by

$$E_1(\vec{r}) = \frac{1}{4\pi} \int d^3\vec{r}' \frac{\exp(ik|\vec{r} - \vec{r}'|)}{|\vec{r} - \vec{r}'|} [2k^2 n_1(\vec{r}') \exp(ikz')]. \quad (32)$$

### 3. The Method of Smooth Perturbations-Rytov Approximation

In addition to the Born approximation, Tatarski develops the Rytov approximation which assumes a solution to equation (30) of the form

$$E = \exp(\Psi) = \exp(X + iS), \quad (33)$$

or simply

$$E = A \exp(iS), \quad (34)$$

where  $A$  is the amplitude given by  $A = \exp X$ . Applying equation (33) to equation (30) and dividing by  $E_0$ , yields the Rytov solution given by.

$$\nabla^2 E + k^2 n^2(r) = \nabla^2 \log E + (\nabla \log E)^2 + k^2 n^2(r). \quad (35)$$

Tatarski further shows that both methods of approximation are equivalent.

### C. HUYGENS-FRESNEL THEORY

As we have seen, the theories of Tatarski and Clifford use the differential equation approach to solve the problem of propagation through a turbulent medium. However, Lutomirski and Yura [Ref. 5], approach this problem in terms of integral equations which use an extended Huygens-Fresnel theory. This technique is equivalent to a differential equation approach, but it is easier to integrate and simulate using FFT tech-

niques. Lutomiński and Yura, develop an extended Huygens-Fresnel theory by introducing a random phase term for turbulence in the Huygens-Fresnel integral which is developed in standard optics texts like [Ref. 6]. This additional phase perturbation takes the form of the Rytov approximation,  $e^\Psi$ . The extended Huygens-Fresnel integral is,

$$E(\vec{r}) = \frac{-ik}{2\pi} \int_S \frac{e(ik|\vec{r} - \vec{r}'|)}{|\vec{r} - \vec{r}'|} E(\vec{r}') e^{i\Psi(\vec{r})} d^2\vec{r}'. \quad (36)$$

In the geometrical optics limit, Fermat's Principle is,  $\Psi \rightarrow k \int n_1(z) dz$ . With a power series expansion of  $e^\Psi$ , equation (36) reduces to the Green's function solution of Tatarski and Clifford given in equation (32).

Recently, Martin and Flatté [Ref. 7] presented an atmospheric turbulence algorithm which uses the differential equation approach that has as a solution, the extended Huygens-Fresnel integral. A filtered random Gaussian phase screen introduces the phase perturbations while the algorithm's path integral method, incorporates a multi-screen transfer function form of Fresnel propagation.

#### D. MUTUAL COHERENCE FUNCTION

The effects of atmospheric turbulence can be expressed in terms of two functions, the Mutual Coherence Function (MCF) and the Modulation Transfer Function (MTF). Lutomiński and Yura [Ref. 5] derive the first concept by considering the average intensity  $\langle I(r) \rangle = \langle E^*(\vec{r}_1) E(\vec{r}_2) \rangle$ , of equation (36). What results is an average intensity which is a product of the autocovariance of the aperture and the atmospheric MCF. The atmospheric MCF term has the Rytov form  $\langle \exp(\Psi''^* + \Psi'') \rangle$  where the  $\Psi''^*$  refers to the complex phase factor at the  $r_1$  coordinate and  $\Psi''$  corresponds to the  $r_2$  coordinate. This term is log-normally distributed, as long as,  $\Psi$  is composed of Gaussian variables. Using this fact and results in Fried's work [Ref. 8], the atmospheric MCF was written in terms of the wave structure function  $D(\rho)$ , given by

$$\langle e^{(\Psi''^* + \Psi'')} \rangle = \exp \left[ \frac{-D(\rho)}{2} \right], \quad (37)$$

where  $D(\rho) = D_x(\rho) + D_s(\rho)$ . Lutomiński and Yura apply the structure function for a plane wave.

$$D(\rho) = 2.91k^2\rho^{5/3} \int_0^L C_n^2(z)dz, \quad (38)$$

to equation (37) which can be written as,

$$\langle e^{(\Psi'^* + \Psi'')} \rangle = MCF(\rho) = \exp\left[-\left(\frac{\rho}{\rho_0}\right)^{5/3}\right], \quad (39)$$

where  $\rho_0$ , the lateral coherence length, given by

$$\rho_0 = [1.46k^2 \int_0^L C_n^2(z)dz]^{-3/5}, \quad (40)$$

where  $k = \frac{2\pi}{\lambda}$  and  $C_n^2$  is the index of refraction structure parameter along the optical path length  $L$ , represents the distance where the spatial coherence of the wave drops to  $e^{-1}$  point of the MCF. [Ref. 8]

## E. MODULATION TRANSFER FUNCTION

Lutomirski and Yura's concept of MCF is closely related to the MTF of Fried's [Ref. 8]. The MCF and MTF are in fact the same function but expressed in terms of different variables. The MCF is measured in the coordinates of the propagation field and has dimensions of distance, while the MTF, is measured in the image plane and has the dimensions of spatial frequency. Both are equivalent under a transformation between the two planes by letting  $\rho \rightarrow \lambda Rf$  where  $R$  is the focal length of the optics and  $f$  is the spatial frequency. This transformation is valid under the Wiener-Khintchine theorem since the lens Fourier transforms the incident electric field at the aperture to the image plane. Fried's expression for the atmospheric long term MTF is

$$MTF(f) = \exp\left[-3.44\left(\frac{\lambda Rf}{r_0}\right)^{5/3}\right], \quad (41)$$

where  $r_0 = 2.1\rho_0$ .

In calculating the MTF, two distinct cases exist. These are a short term and long term MTF. The short term exposure describes the evaluation of the wavefront in sufficiently short time intervals such that the turbulence appears frozen. The long term

MTF, is a single long time integrated exposure, taking into account every turbulence configuration. This thesis focuses on the method prescribed by the short term MTF. [Ref. 8]

The analytic distinction between the two cases lies in the manner in which the wavefront distortions are handled. Specifically, the distortion attributed to a random tilt of the wavefront. Tilt results from the varying phase fluctuations across the aperture which accumulate along the optical propagation path. These fluctuations produce image motion in the focal plane of the receiver. For a very short exposure, the tilt is extracted, by fitting a mean square two-dimensional flat plane to the electric field and rotating it through an angle so that the mean wavefront is normal to the direction of propagation. This introduces a phase shift, resulting in the displacement of each curve about the optical axis. Fried's [Ref. 8] development of this theory suggests a higher MTF at all spatial frequencies for the short term MTF. The short-exposure MTF for near-field and far-field cases is respectively given by

$$\begin{aligned} \langle \tau_0(f) \rangle_{nf} &= \tau_0(f) \exp \left[ -3.44 \left[ \frac{\lambda R f}{r_0} \right]^{5/3} \left[ 1 - \left[ \frac{\lambda R f}{D} \right]^{1/3} \right] \right], \\ \langle \tau_0(f) \rangle_{ff} &= \tau_0(f) \exp \left[ -3.44 \left[ \frac{\lambda R f}{r_0} \right]^{5/3} \left[ 1 - \frac{1}{2} \left[ \frac{\lambda R f}{D} \right]^{1/3} \right] \right]. \end{aligned} \quad (42)$$

where  $\tau_0$  is the MTF of a diffraction-limited lens, and the exponential term corresponds to the atmospheric MTF. These equations predict a near field short term MTF that start at one, declines to a minimum, then increases to unity, at the optical cut off frequency. Figure 1 illustrates this phenomena.

## F. DIFFRACTION INTEGRAL

This section presents the analytical work concerned with the development of my propagation algorithms. It begins by illustrating the approximations that were used to manipulate the diffraction integral and then proceeds with the analysis required to transform the solution of the Helmholtz equation into two forms of the Huygens-Fresnel principle. The two forms are, first, a convolution form suited for long distance propagation and second, as a transfer function form for short distance propagation. Some initial assumptions made by Roberts [Ref. 9] include the following:

1. Light propagates in the  $k$  direction.
2. The wave amplitude is known in the  $xy$ -plane at  $z = 0$ .

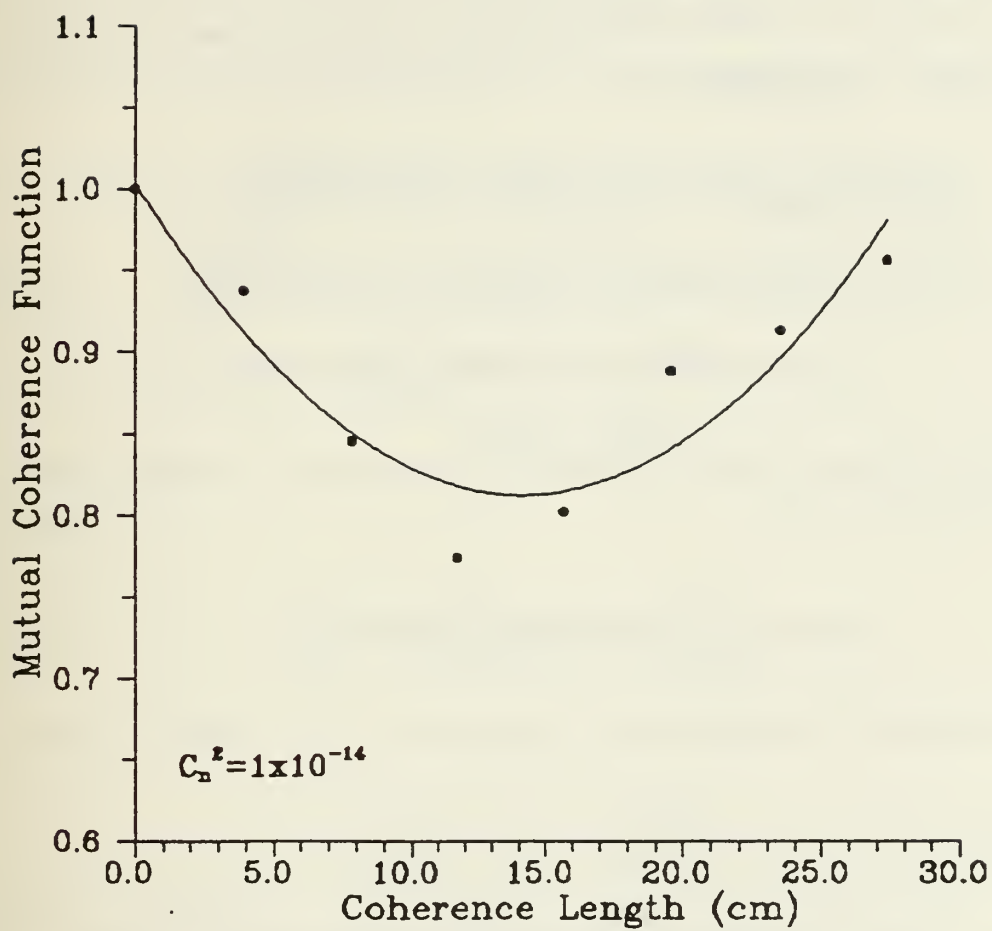


Figure 1. Short Term Mutual Coherence Function for an 8 x 8 Subaperture.

3. Polarization effects are negligible.
4. The electric field amplitude is a scalar function  $V(r,z)$ .

Following Roberts, the analysis begins with the Huygens-Fresnel integral for the propagation of light waves given as

$$V(\bar{r}, z) = \frac{-i}{\lambda z} \int d\bar{\rho} V(\bar{\rho}, 0) \exp\left[ \frac{2\pi i}{\lambda} \sqrt{z^2 + |\bar{r} - \bar{\rho}|^2} \right], \quad (43)$$

where  $\lambda$  is the wavelength of light and  $\bar{\rho}$  is a vector in the aperture plane,  $\bar{r}$  is a vector in the image plane, and  $z$  is the propagation direction. From the Fresnel approximation where,  $r \ll z$  and  $\rho \ll z$ , factor  $z^2$  from the square root and expand by a binomial expansion. Equation (43) becomes

$$\begin{aligned} V(\bar{r}, z) &= \frac{-i}{\lambda z} \int d\bar{\rho} V(\bar{\rho}, 0) \exp\left[ \frac{2\pi i z}{\lambda} \sqrt{1 - \left| \frac{\bar{r} - \bar{\rho}}{z} \right|^2} \right], \\ &\simeq \frac{-i}{\lambda z} \int d\bar{\rho} V(\bar{\rho}, 0) \exp\left[ \frac{-2\pi i z}{\lambda} \left( 1 - \frac{1}{2} \left| \frac{\bar{r} - \bar{\rho}}{z} \right|^2 \right) \right], \\ &\simeq \frac{-i}{\lambda z} \exp\left( \frac{-2\pi i z}{\lambda} \right) \int d\bar{\rho} V(\bar{\rho}, 0) \exp\left( \frac{i\pi}{\lambda z} |\bar{r} - \bar{\rho}|^2 \right). \end{aligned} \quad (44)$$

Since the exponential phase factor outside of the integral does not affect intensity measurements, equation (44) is

$$V(\bar{r}, z) \simeq \frac{-i}{\lambda z} \int d\bar{\rho} V(\bar{\rho}, 0) \exp\left[ \frac{i\pi}{\lambda z} |\bar{r} - \bar{\rho}|^2 \right]. \quad (45)$$

Expanding the quadratic term gives,

$$\begin{aligned} V(\bar{r}, z) &= \frac{-i}{\lambda z} \int d\bar{\rho} V(\bar{\rho}, 0) \exp\left[ \frac{i\pi}{\lambda z} [r^2 - 2\bar{r} \cdot \bar{\rho} + \rho^2] \right], \\ &= \frac{-i}{\lambda z} \exp\left[ \frac{i\pi}{\lambda z} r^2 \right] \int d\bar{\rho} V(\bar{\rho}, 0) \exp\left[ \frac{i\pi}{\lambda z} \rho^2 \right] \exp\left[ -2\pi i \left[ \frac{\bar{\rho} \cdot \bar{r}}{\lambda z} \right] \right]. \end{aligned} \quad (46)$$

This is the convolution form of the Fresnel integral, which is equivalent to the Fraunhofer integral except for the quadratic phase factor in the integral.

To obtain the transfer function form, the analysis begins with denoting  $\tilde{V}(f,z)$  as the Fourier transform of  $V(r,z)$  given by

$$\tilde{V}(\tilde{f}, z) = \int \int d\tilde{r} \exp(-2\pi i \tilde{f} \cdot \tilde{r}) V(\tilde{r}, z), \quad (47)$$

where  $V(\tilde{r}, z)$  is given in equation (45). Interchanging the order of integration yields

$$\tilde{V}(\tilde{f}, z) = \frac{-i}{\lambda z} \int d\bar{\rho} V(\bar{\rho}, 0) \int d\tilde{r} \exp(-2\pi i \tilde{f} \cdot \tilde{r}) \exp\left[\frac{i\pi}{\lambda z} |\tilde{r} - \bar{\rho}|^2\right]. \quad (48)$$

Next, a change of variables is made where

$$\tilde{r}' = \tilde{r} - \bar{\rho}. \quad (49)$$

Substituting this into equation (48) gives the following equation

$$\begin{aligned} \tilde{V}(\tilde{f}, z) &= \frac{-i}{\lambda z} \int d\bar{\rho} V(\bar{\rho}, 0) \int d\tilde{r}' \exp[-2\pi i \tilde{f} \cdot (\tilde{r}' + \bar{\rho})] \exp\left[\frac{i\pi}{\lambda z} r'^2\right], \\ &= \frac{-i}{\lambda z} \int d\bar{\rho} V(\bar{\rho}, 0) \exp(-2\pi i \tilde{f} \cdot \bar{\rho}) \int d\tilde{r}' \exp(-2\pi i \tilde{f} \cdot \tilde{r}') \exp\left[\frac{i\pi}{\lambda z} r'^2\right]. \end{aligned} \quad (50)$$

The  $r'$  integral is replaced with its Gaussian transform pair,

$$i\lambda z \exp(-i\pi\lambda z f^2), \quad (51)$$

giving

$$\tilde{V}(\tilde{f}, z) = \exp(-i\pi\lambda z f^2) \int d\bar{\rho} V(\bar{\rho}, 0) \exp(-2\pi i \tilde{f} \cdot \bar{\rho}). \quad (52)$$

The inverse Fourier transform of equation (52) yields

$$V(\tilde{r}, z) = \int d\tilde{f} \exp(2\pi i \tilde{f} \cdot \tilde{r}) \exp(-i\pi\lambda z f^2) \int d\bar{\rho} V(\bar{\rho}, 0) \exp(-2\pi i \tilde{f} \cdot \bar{\rho}). \quad (53)$$

This expression is the transfer function form of the diffraction integral, which is equivalent to the solution of the differential equation approach used by Martin and Flatté [Ref. 7]. Reviewing the form of equations (46) and (53), the need for two equations describing different propagations, is obvious. In one instance, the propagation distance  $z$  enters in the denominator of the exponential term. It is at long distances that the exponential term varies slowly. On the other hand, equation (53) is suited for short

propagation distances, as  $z$  enters into the numerator of the exponential for slow variations in this case.

### III. NUMERICAL SIMULATION MODEL

This numerical simulation, modeled wave optics propagation of an electromagnetic wave through a random medium, represented by a two-dimensional Gaussian phase screens. Techniques in this model required certain "tools" and their testing. These "tools" included a need for a reliable random number generator, used in generating the random phase screens, and an efficient two-dimensional FFT, used in approximating the diffraction integrals. But first, a discussion of the experimental arrangement is needed.

#### A. EXPERIMENTAL ARRANGEMENT

Due to the extensive numerical calculations in this simulation, a Compaq deskpro 80386-20 computer was used. It features a 64 megabyte hard drive and 16 megabytes of memory. In addition to the 20-MHz 80387 coprocessor, a Weitek 1167 math coprocessor was added to enhance execution speed. The 32 bit Fortran-386 compiler was from Silicon Valley Software (SVS) and uses Phar Lap Software to extend the operating system beyond one megabyte. The math and graphics packages were produced by Scitech Scientific. The Compaq has a 640 x 480 pixel VGA graphics monitor. Both the HP Laser Jet Series II and Panasonic KX-P1092i multi-mode printers were used in this arrangement.

#### B. COMPUTER PRELIMINARIES

##### 1. Random number generator

The main purpose of a computer simulation is to approximate natural phenomena. To make things realistic, random number sequences were used to introduce stochastic variations. One might ask, what minimal criteria should a particular random number generator satisfy? Certainly the most important criterion is that the sequence of numbers is sufficiently random. Other criteria are uniformity, reproducibility, minimum memory, fast, non-repeating, and statistically independent.

The more difficult characteristic to satisfy is statistical independence. Thus a series of tests were needed to provide a quantitative measure of the generator's performance. There are two kinds of statistical tests: empirical tests and theoretical tests. Empirical tests focus on how the computer manipulates groups of numbers from the sequence and evaluates certain statistical quantities. Perhaps the best known of all sta-

tistical tests are the "Chi-Square" tests. Theoretical tests, on the other hand, establish characteristics of a sequence using methods based on recurrence rules. [Ref. 10]

For the purpose of this simulation, only empirical tests were applied to the SVS-Fortran random number generator called *Ran/I*. The following five tests were considered:

1. Frequency Test. This test determines whether or not the sequence of numbers are uniformly distributed as  $U(0,1)$ .
2. Serial Test. This test is an extension of the frequency test to two dimensions or matrix form.
3. Lagged-Product Test. This test checks for correlations between successive numbers over a given lag period.
4. Run Tests:
  - a. Runs up and down. This tests for long increasing and decreasing sequences of numbers.
  - b. Runs above and below the mean. This tests for long sequences with values consistently above or below the mean.

The results of the five tests are provided in Appendix A. Of these five tests, the Lagged-Product and Runs Tests are the most critical when simulating atmospheric turbulence. These three tests determine whether or not correlation is introduced from the random number generator which produces erroneous results in the simulation. The SVS-Fortran random number generator met the test criteria and proved to be one of the better generators. However, this generator has one significant draw back. The random sequences begin at one of two different values depending on whether the seed value is positive or negative. Thus it is critical that the random numbers be called continuously in a loop to avoid restarting the sequence, thereby introducing unwanted correlation.

## 2. Fast Fourier Transform

The most repeatedly used algorithm throughout the numerical simulation was the fast fourier transform. Therefore, it was necessary to use the most efficient algorithm available. The Scitech Scientific math package provided several options, with subroutine *FFT2C*, best suited for this numerical simulation. This subroutine uses a complex array input. The other FFT considered was a routine coded by Dr. Walters which he received in a demonstration package provided by Infotek. This FFT utilizes real arrays and will henceforth be referred to as subroutine *FFT*.

Each subroutine was timed for various configurations. Specific timing results are contained in Appendix B. Some general results, however, are that subroutine

*FFT2C* was faster for one-dimensional cases, with subroutine *FFT* faster for the two-dimensional cases. The decline in efficiency of *FFT2C* can be attributed to the extra coding required to convert between real arrays and complex arrays. Subroutine *FFT* was selected over *FFT2C* since the simulation utilized the two-dimensional form of the FFT.

Other techniques which were employed to increase the efficiency included installing a Weitek coprocessor in the Compaq. This reduced the processing time to approximately one-third that of the original time. The use of common blocks vice dimension statements further decreased processing time by 5%. Finally, a portion of the FFT algorithm was modified from  $wim = \sin(ang)$  , to  $wim = \sqrt{1 - wre^2}$  , with a negligible decline in efficiency by 0.01%.

Because of the discrete nature of the simulation, there exists problems and limitations associated with implementating the FFT. One such problem was that of classical edge diffraction associated with the phase or amplitude discontinuities at the edges of the finite screen. As the propagation distance  $z$  increases, the edge diffraction spreads toward the center of the screen making more and more of the diffraction pattern erroneous. Buckley [Ref. 11] defines the distance from the ends of the screens where the edge diffraction is important as

$$D(z) = 2\sqrt{\pi z} + 2\phi_0\pi z, \quad (54)$$

where  $z$  is the propagation distance and  $\phi_0$  is the root mean square phase deviation imposed on the wave by the screen. The severity of edge effects, however, is reduced by the aliasing introduced in the FFT implementation. Aliasing transforms the linear screen to a "circular" one with the last point associated with the first. This results in a continuity of phase and amplitude at the edges of the screen [Ref. 11].

The most important limitation was the finite spatial range imposed by the maximum available grid size. This places a constraint on the available range of frequencies used in the FFT from the lowest given by  $f_{min} = 1/L$  , to the highest,  $f_{max} = n/2L$ , where  $L$  is the grid length and  $n$  is the number of grid points. Figure 3 on page 20 illustrates this setup. The FFT provides a least squares fit of sine and cosine fuctions to the perturbed wavefront phases. However, this method prevents an accurate representation of the wavefront at low frequencies for a Kolmogorov  $\kappa^{-11/3}$  power spectrum. To alleviate this problem, a subaperture was superimposed at the center of the grid. The subaperture helps low frequencies, which contain a large portion of the am-

plitude, but hurts the high frequencies by limiting the inner scale. There exists some high frequency edge effects, however, these are minimal.

### C. PROCEDURE

Figure 2 provides a summary of the coding contained in Appendix C. This conceptual diagram illustrates an overview of the procedural steps of the Fraunhofer propagation algorithm.

#### 1. Input Parameters

Since this step is straightforward, extensive discussion is not required. However, it is important to note that the input parameters were both fixed and variable. The array size and filter value were fixed quantities, but the subaperture size, seed value,  $C_n^2$  value, and propagation distance, took on different values. The actual variable names are documented at the beginning of the code.

#### 2. Aperture Mutual Coherence Function

The second step in this procedure calculates the aperture MCF. Subroutine *MCF* does this. In this subroutine the initial wavefront was represented in the computer as an  $L \times L$  square array of complex numbers. Centered within this complex electric field was a subaperture. The initial complex electric field had a value of zero, everywhere, except for the real part of the subaperture, which had the value of one. Figure 3 illustrates this. With the electric field created, it was direct Fourier transformed (DFT) by subroutine *DFTIFT*. The intensity of the electric field was calculated, and then inverse Fourier transformed (IFT), yielding the aperture MCF.

#### 3. Planar Electric Field

The complex electric field was created by the same method prescribed in subroutine *MCF*. It is important to realize that the concept of aperture size was used in two ways. One way corresponds to the simulated aperture while the other pertains to an aperture with physical dimensions. The simulated aperture is actually a matrix or grid which directly reflects the dimensioning size. For example, the simulated  $L \times L$  complex electric field was actually a two-dimensional matrix corresponding to a  $256 \times 256$  two-dimensional array. From the input parameters, the simulated subaperture takes on grid sizes ranging from an  $8 \times 8$  to  $200 \times 200$  square matrix.

The second referencing to an aperture refers to an aperture with actual physical units. The physical subaperture was assigned a value of 0.3125 meters, which remains fixed regardless of the simulated subaperture size. The length  $L$  of the complex electric

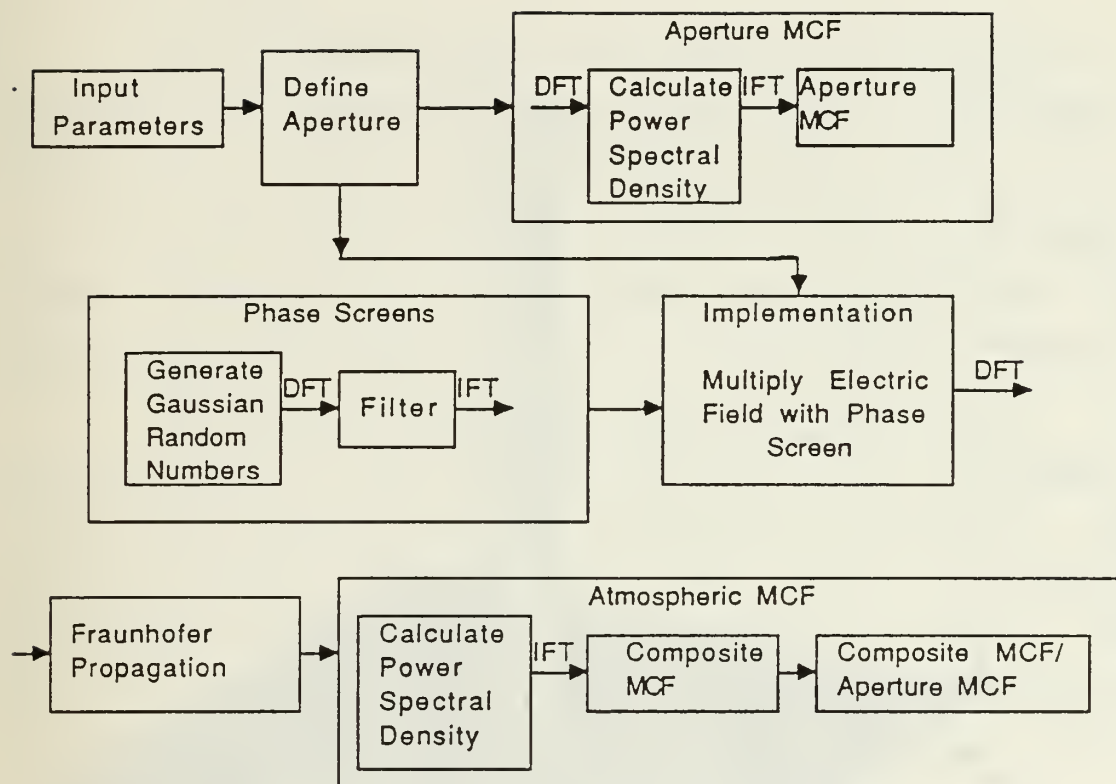


Figure 2. Conceptual Diagram of the Simulation Coding.

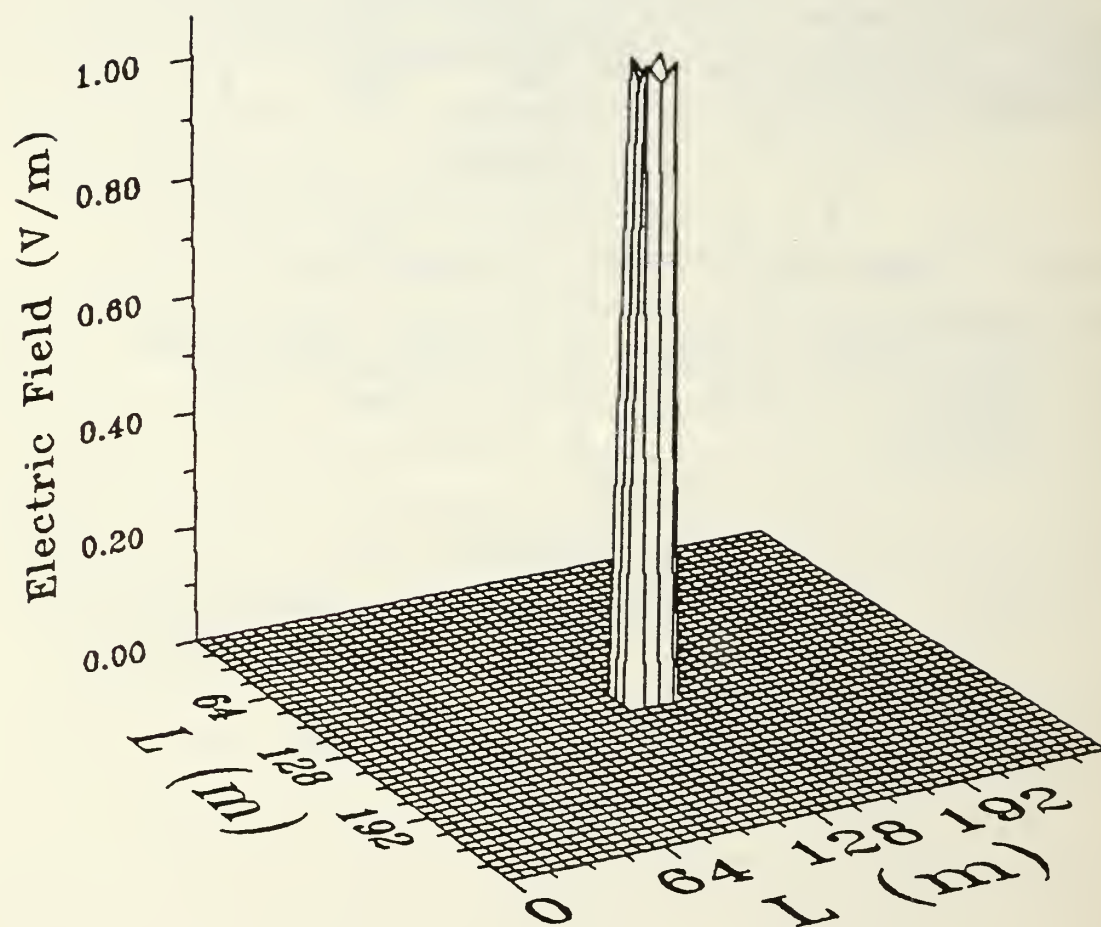


Figure 3. Three Dimensional Perspective of the Initial Electric Field.

field, on the other hand, had variable physical lengths depending on the simulated supaperture size. The physical value of  $L$  was calculated from

$$L = m \times \frac{nr}{isize} [\text{meters}], \quad (55)$$

where  $m$  is the physical subaperture length in meters,  $nr$  is the integer value of the array dimensioning, and  $isize$  is the integer value for the simulated subaperture.

#### 4. Phase Screens

##### a. Generation

Phase screens were created in subroutine *GGAUS* by constructing a  $L \times L$  matrix of Gaussian distributed random numbers. Each position was assigned an independent random number  $n$ , thereby, requiring  $n^2$  random numbers. Since the SVS-Fortran random number generator was uniformly distributed, an algorithm provided by Knuth [Ref. 10] transformed the distribution into a Gaussian one. Two independent, two-dimensional real arrays called *phaser* and *phasei* were created, which represent the real and imaginary components of a two-dimensional complex phase screen. In this algorithm, the imaginary part of the phase screen was set to zero.

The domain in which the phase screens are created is arbitrary, however, filtering was done in the Fourier plane. Creating the phase screen in frequency space vice real space, reduces the requirement for an additional FFT when transforming from real space to frequency space. Martin and Flatté [Ref. 7] proposed this method, but it creates difficulties in absolute normalization. Further discussion is presented in Chapter four. This simulation, on the other hand, generated the random Gaussian phase screen in real space. This in turn was DFT'd to frequency space where the complex phase screen was filtered and then the filtered phase screen was IFT'd.

##### b. Filtering

Phase screens were filtered to obtain the correct power law form. The filtering function used in subroutine *FLTR* was,

$$\Phi_0(\kappa) = 2\pi k^2 \delta_x \Phi_n, \quad (56)$$

where  $\delta_x$  is the slab thickness and  $\Phi_n = 0.033 C_n^2 \kappa^{-11/3}$ , which gives the relationship between the phase spectrum and refractive-index spectrum [Ref. 2, pp. 101-102.]. Filtering was accomplished by multiplying each phase screen spectrum by the square root of equation (56). The correct filtering method requires circular frequency filtering instead of a linear one, because of two-dimensional isotropy. The correct form is

$\kappa = \sqrt{\kappa_x^2 + \kappa_y^2}$ , which is radial everywhere except at the origin, where it is zero [Ref. 12]. This was reflected in the simulation by setting the position (1,1) equal to zero in each two-dimensional real array which makes up the complex phase screen.

It is important to realize that although the filtering concept is simple and straightforward, the actual implementation is not. The difficulty arises from the symmetry properties of the digitally filtered phase screen.

A one-dimensional case offers a simple illustration of this concept. The FFT of a complex function which contains only real components, results in a symmetric function in frequency space about the Nyquist frequency for the real components, and an anti-symmetric function for the imaginaries. With these symmetries present in the frequency domain, the correct implementation of the filtering is to mimic these symmetries. Thus a "folding" technique about the Nyquist frequency was required. However, when this concept was extended to a two-dimensional case, as in the phase screen in the simulation, the symmetries imposed by the FFT, were no longer apparent in the frequency domain. To simplify the symmetry requirements, a real phase screen was used. The real and imaginary spectral components were filtered by folding about the Nyquist frequency. It was suggested by both Brigham [Ref. 13] and Martin and Flatté that a complex phase screen containing both real and imaginary components, yields two entirely distinct phase screens. However, nothing was provided to support this hypothesis.

Another important consequence of filtering resides in the units. The phase screens were filtered in  $\kappa$  units, but the FFT algorithm operates in frequency units. Therefore, it was necessary to make a change of variables prior to applying the IFT. The relationship used for the change of variables is  $\kappa = 2\pi v$ .

The paper by Martin and Flatté [Ref. 7], specifies an additional normalization factor of  $\Delta_k^{-1}$  in equation (56), where  $\Delta_k = \frac{2\pi}{N\Delta}$  and where  $N$  is the number of grid points and  $\Delta$  is the sampling interval. Martin and Flatté provided no explanation for the additional  $\Delta_k^{-1}$  in the filtering. It was not included in the filtering code.

## 5. Implementation

After the filtered phase screen was IFT'd into real space, it was introduced into the code as a phase screen and multiplied with the electric field. The array *phaser*, which contains the desired phase field, takes the form of the Rytov approximation,  $e^{i\theta}$ , in the extended Huygens-Fresnel integral. This form assumes that only phase perturbations and not amplitude variations, occur.

## 6. Propagation Methods

As indicated in previous sections, the Huygens-Fresnel technique was used to simulate the propagation of light. This was accomplished by applying the FFT to the perturbed electric field. Both the "far-field" and "near-field" propagation methods were considered.

### *a. Fraunhofer*

Of the two different propagation methods, the single screen Fraunhofer propagation is by far the simplest technique to implement and the one implemented in this thesis. The uniform coherent plane wave at the aperture was FFT'd yielding the desired diffraction pattern. Looking more closely, one can see that under certain circumstances, Fraunhofer propagation is just a special case of the long distance convolution form of Fresnel propagation given by equation (46). There exists two situations when this occurs. One is a "far-field" case for large distances, where the point of observation is at infinity. The other case, is when a spherical curvature is placed on the wave at the aperture. This curvature cancels the quadratic phase factor in the Fresnel form, at the focal point.

Both Fresnel and Fraunhofer algorithms were needed for propagation. It was essential to verify and validate each case before building on the pre-existing codes. The Fraunhofer algorithm provided the basis of this simulation. Since the Fraunhofer diffraction pattern is well-known, it provided a means to verify the existing code by comparing the simulated diffraction pattern with theoretical results. Figure 4 and Figure 5 illustrate one three-dimensional quadrant of the diffraction pattern of an unperturbed electric field, for two different subaperture sizes. While Figure 6 illustrates one three-dimensional quadrant of a perturbed electric field diffraction pattern for a 16 x 16 subaperture.

### *b. Fresnel*

Although the Fresnel propagation forms were implemented but not tested in this thesis, discussion is warranted since multi-screen Fresnel propagation is predominantly used in thermal blooming and multiple scattering scenarios. Propagation through the turbulent boundary layer also requires Fresnel propagation codes. Two different forms are used for Fresnel propagation, which apply a straightforward FFT to evaluate them. These two forms however, do not allow for a variable receiving array size. In addition, choosing the correct number of sample points is essential. An effective approach used to resolve these problems is the Fresnel number.

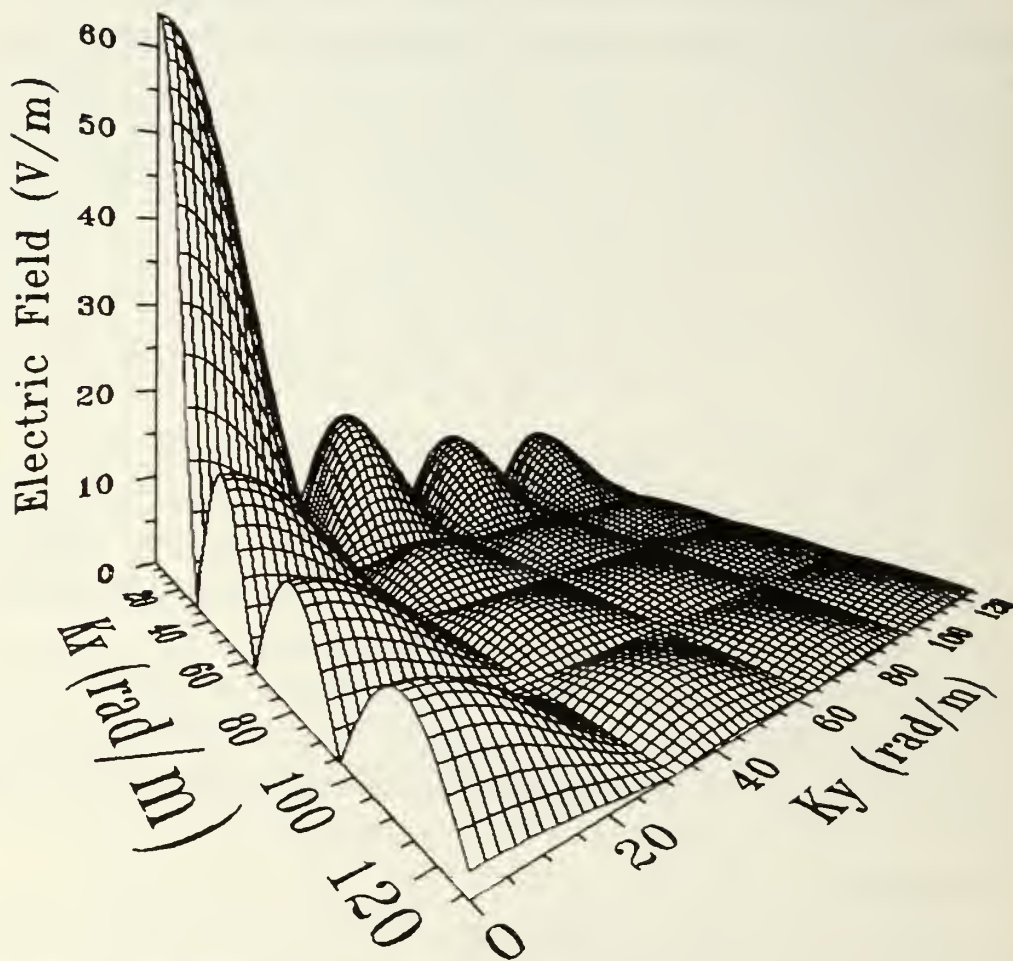


Figure 4. Three Dimensional Diffraction Pattern for an 8 x 8 Subaperture.

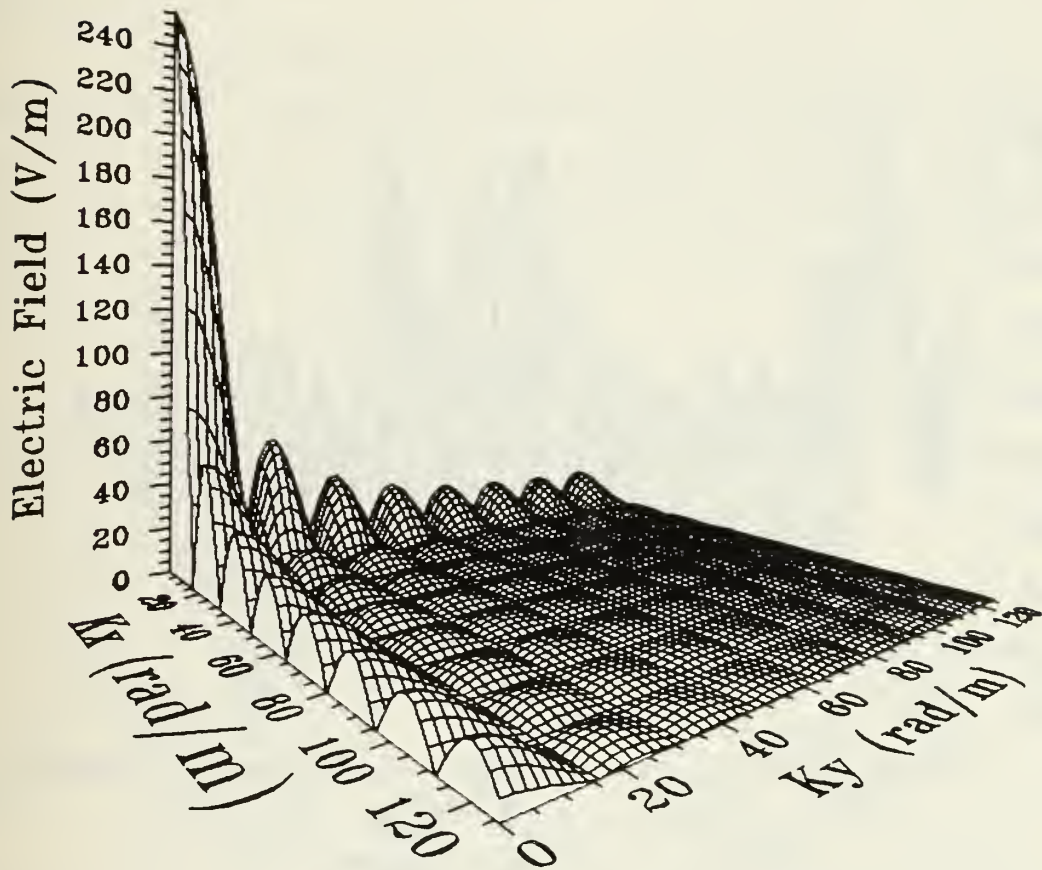


Figure 5. Three Dimensional Diffraction Pattern of a 16 x 16 Subaperture.

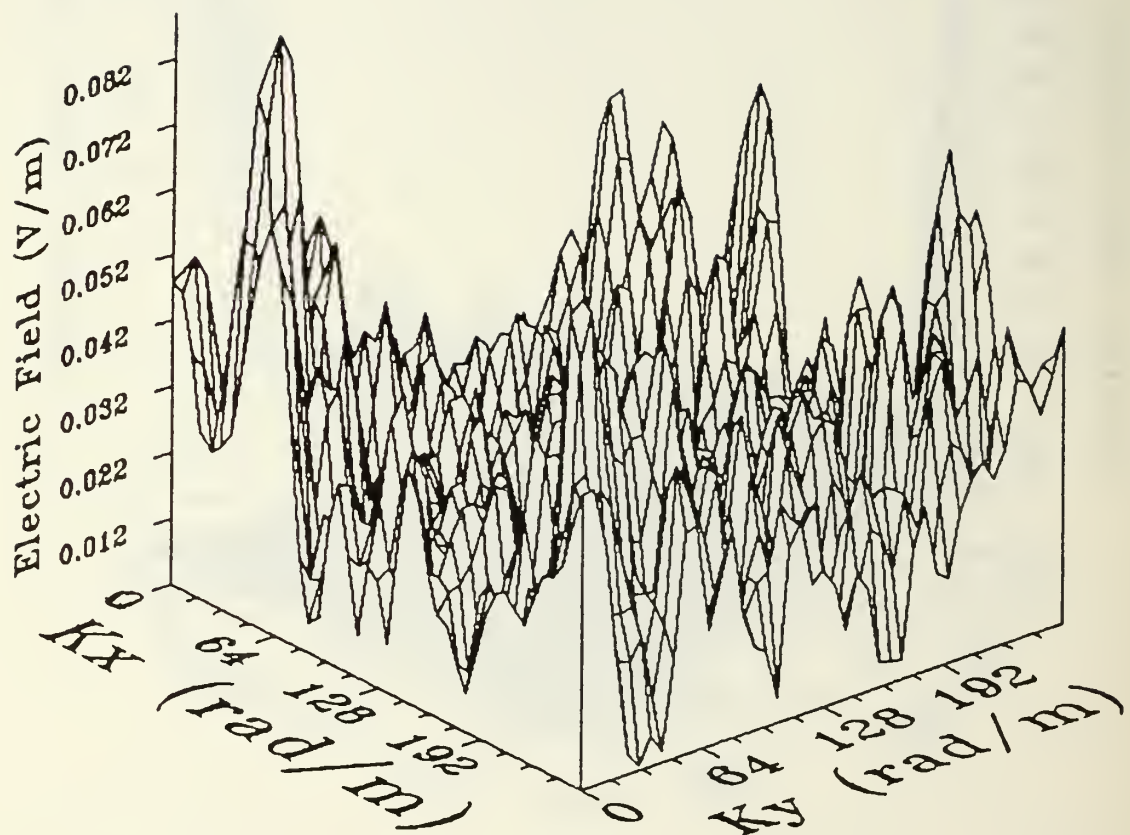


Figure 6. Perturbed Diffraction Pattern of a 16 x 16 Subaperture.

The Fresnel number is

$$N_f = \frac{\Delta r \Delta \rho}{\lambda z}, \quad (57)$$

where  $\Delta r$  is the receiving aperture size,  $\Delta \rho$  is the transmitting aperture size,  $\lambda$  is the wavelength of light, and  $z$  is the propagation distance. Implementation of the correct Fresnel form depends on the Fresnel number. When the Fresnel number is smaller than the number of grid points in the field length, that is,  $N_f \leq N$ , the long distance propagation algorithm is used. Conversely, when  $N \geq N_f$ , the short distance code is implemented.[Ref. 14]

The long distance propagation code uses the convolution form of the diffraction integral. Implementation requires placing a curvature on the electric field wavefront at the aperture. The subroutine called *quad1*, does this. Multiplying the phase screen with the electric field, gives a perturbed electric field that propagates the entire distance by means of one FFT. In the Fourier plane, the quadratic phase factor called *quad2* scales the electric field.

The transfer function form, on the other hand, is suited for short distances. In this case, the entire propagation distance is divided into equally spaced slabs. Two FFT's are required to propagate the distance of each slab. This is accomplished by the following method:

1. Mesh the electric field and phase screen.
2. Apply the direct FFT.
3. Multiply the field by the propagation transfer function subroutine called *trnsfr*.
4. Apply the inverse FFT.

This procedure is repeated for each phase screen until the observing plane is reached. [Ref. 7]

Both forms of Fresnel propagation were included in the simulation code contained in Appendix C, however, neither form of Fresnel propagation was exercised.

## 7. Atmospheric Mutual Coherence Function

The final step in this simulation calculated the atmospheric MCF. The same procedure used to calculate the aperture MCF, was applied to the perturbed electric field, with one exception. The difference is that division of the composite atmospheric-optical MCF by the aperture MCF, gives the atmospheric MCF.

## IV. RESULTS

The main objectives of this thesis were to demonstrate that the simulation gives results that provide insight to weak scattering wave propagation and examine the accuracy of the simulation code. The limitations imposed by the computer mechanics and the actual method of implementing turbulence theory are discussed. Specific areas of interest include the filter function, MCF, and saturation effects.

### A. FILTERING

As previously mentioned in chapter three, Martin and Flatté proposed a very different approach to creating the random Gaussian phase screen. Their method suggests creating the phase screen in frequency space, vice real space, to reduce the required number of FFT's from two to one. Since the domain in which the phase screen is generated, is arbitrary, this approach seems plausible. However, this method proved to be awkward. As the subaperture size was successively doubled, it was necessary to increase the strength of turbulence,  $C_n^2$ , by a factor of ten each time, in order to produce the identical level of turbulence as in the previous phase screen. Additionally, since the phase screen was created in frequency space, and no symmetries were present, the filtering technique did not reflect any folding about the Nyquist frequency. It is not clear that aliasing was accounted for in the Martin and Flatté algorithm. Hence, the IFT of the phase screen appears to result in a statistically incorrect phase screen. Additionally, it is not clear how, with one FFT, Martin and Flatté handled the  $2\pi$  and  $1/N$  normalization requirements. With a round trip of FFT's, the normalization problems are automatically handled. The weakly filtered phase screen, in turn, led to MCF curves which grossly overestimated the coherence length,  $\rho_0$ . These problems obtained from Martin and Flatté's approach to simulating turbulence led to the current coding which created one phase screen in real space and applied a folding about the Nyquist frequency, in the filtering, to account for the symmetries introduced by the FFT's.

Kolmogorov theory of atmospheric turbulence predicts that the graph of the phase screen power spectral density versus  $\kappa$  yield a slope of  $-11/3$ . Figure 7 shows that equation (56) produced a filtered phase screen that reflects the  $-11/3$  slope, as well as, the correct folding technique. Identical slopes were expected for all subapertures, as well as, all possible angles which reflect the circular filtering. Other subaperture profiles show a consistent slope value of  $-11/3$ . Figure 8 corresponds to a  $32 \times 32$  subaperture at a

45 degree angle while Figure 9 is representative of a 64 x 64 subaperture at a 90 degree angle. Isotropy is apparent in that the circular filtering was implemented correctly within the error introduced by the randomness in the screen and the ability to linearly fit a line through the data points.

## B. MCF

The MCF of the electric field provides one method of analyzing the accuracy of the simulation. To verify that the MCF was correctly computed, the aperture MCF of an unperturbed electric field was calculated. This was easily accomplished since the image intensity and aperture MCF are transform pairs and are analytical for simple square and circular apertures. The aperture MCF is just the autocorrelation of the aperture function which is evaluated by calculating the area of overlap of two identical apertures as they are moved laterally apart. For a square subaperture, the autocorrelation yields the triangle function, with maximum value of 1.0 and minimum value of 0.0 corresponding directly to the subaperture size. Figure 10 illustrates the MCF, or autocorrelation, of an 8 x 8 and 16 x 16 square subaperture.

The MCF corresponding to the atmospheric turbulence was determined by dividing the MCF of the perturbed electric field by the aperture MCF. The value of  $\rho_0$ , the spatial coherence length, was determined from the turbulence MCF curve. Figure 11 illustrates a simulated  $\rho_0$  value of 3.20 mm for a 64 x 64 subaperture with  $C_n^2 = 1 \times 10^{-13}$ . The theoretical value calculated from equation (40) yields  $\rho_0 = 2.41 \text{ mm}$ . Although the 64 x 64 subaperture gave accurate results other subaperture configurations did not. When  $C_n^2$  increased, the MCF curves fell off rapidly towards zero for all subapertures. Figure 12 illustrates this for a 64 x 64 subaperture. All subaperture configurations were run for two different  $C_n^2$  values. The simulated  $\rho_0$  values were plotted against the corresponding subapertures for each case. Figure 13 reflects the  $C_n^2 = 1 \times 10^{-13} \rho_0$  values, and Figure 14 is for  $C_n^2 = 1 \times 10^{-14}$ . The desired trend is for the simulated  $\rho_0$  values to approach the theoretical value as the subaperture size increased. This trend is visible in Figure 13 where  $C_n^2 = 1 \times 10^{-13}$  and  $\rho_0 = 2.4 \text{ mm}$ . However, Figure 14 shows continuously decreasing  $\rho_0$  values past the theoretical value of 9.6 mm. The results of figures thirteen and fourteen point to a problem that may involve edge effects or aliasing, resulting from undersampling. The  $\rho_0$  values, which were on the order of millimeters, were smaller than the tens of centimeter distances of the subaperture mesh size.

In an attempt to pinpoint the problem, the simulation code was changed to increase the number of frequencies in the subaperture by using a 512 x 512 array. The results

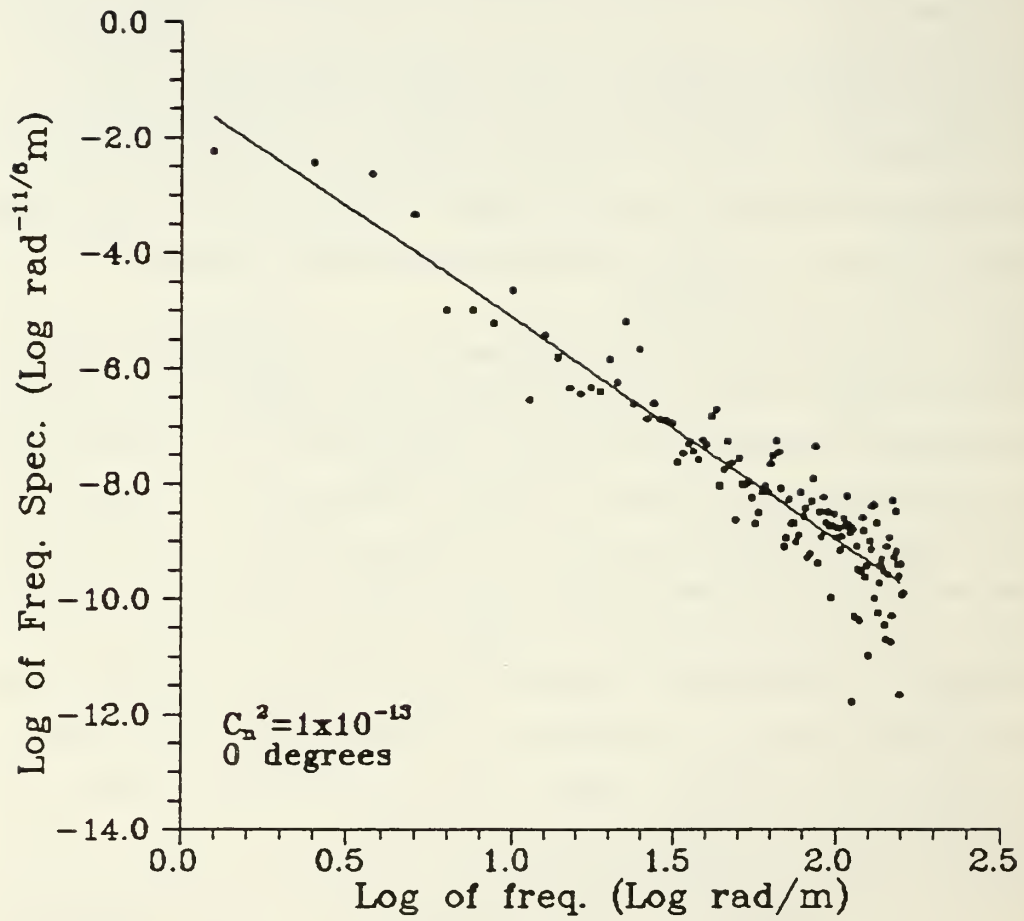


Figure 7. Filtered Phase Screen of a 16 x 16 Subaperture.

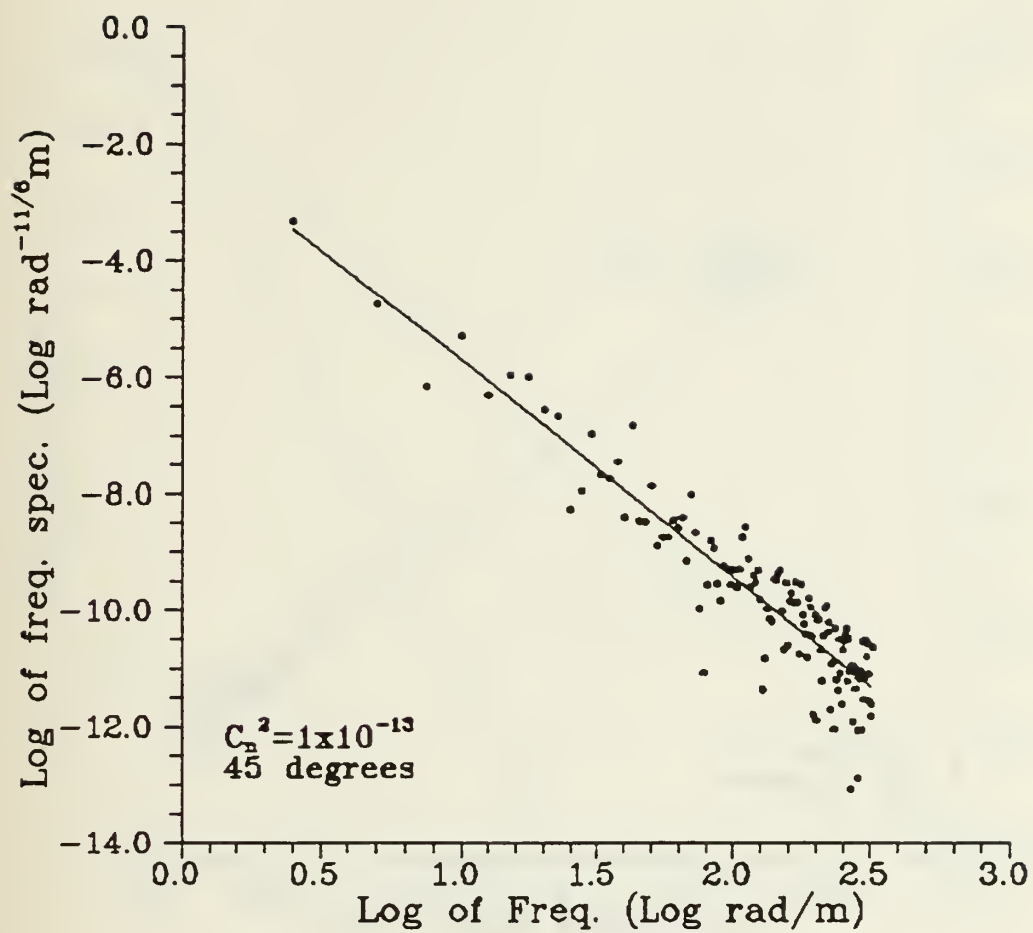


Figure 8. Filtered Phase Screen of a 32 x 32 Subaperture.

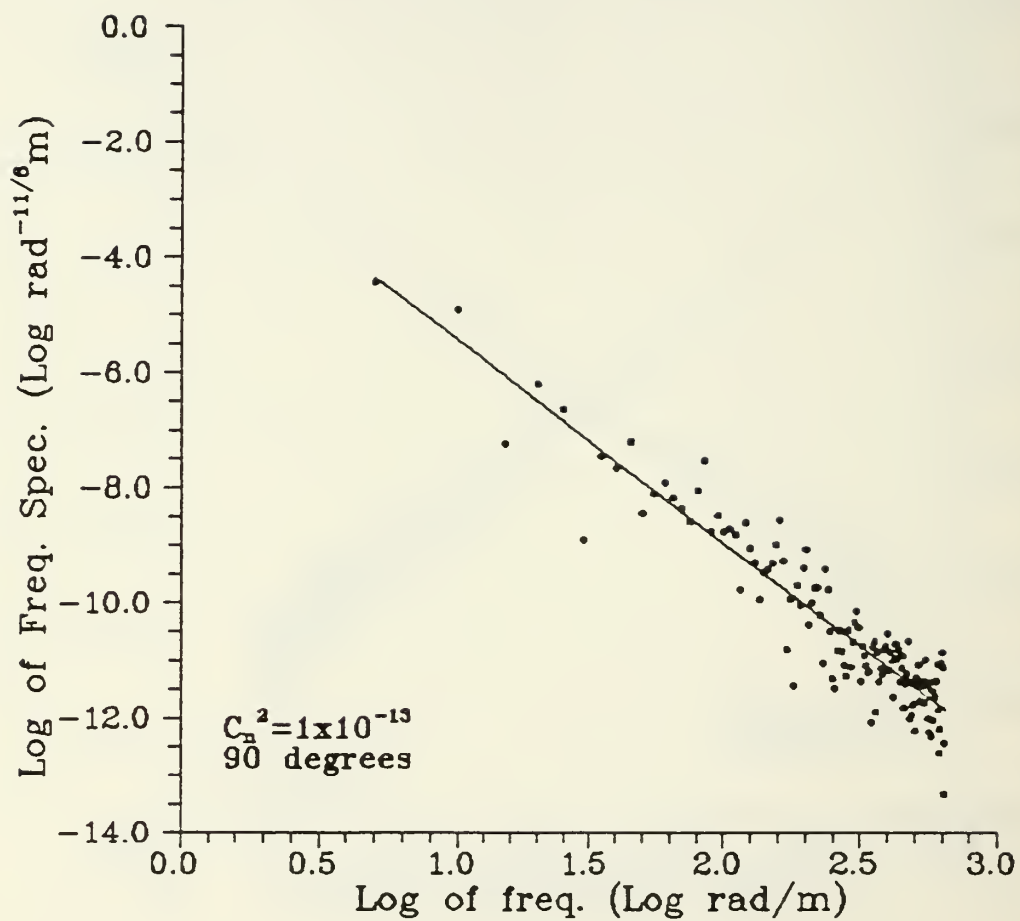


Figure 9. Filtered Phase Screen of a 64 x 64 Subaperture.

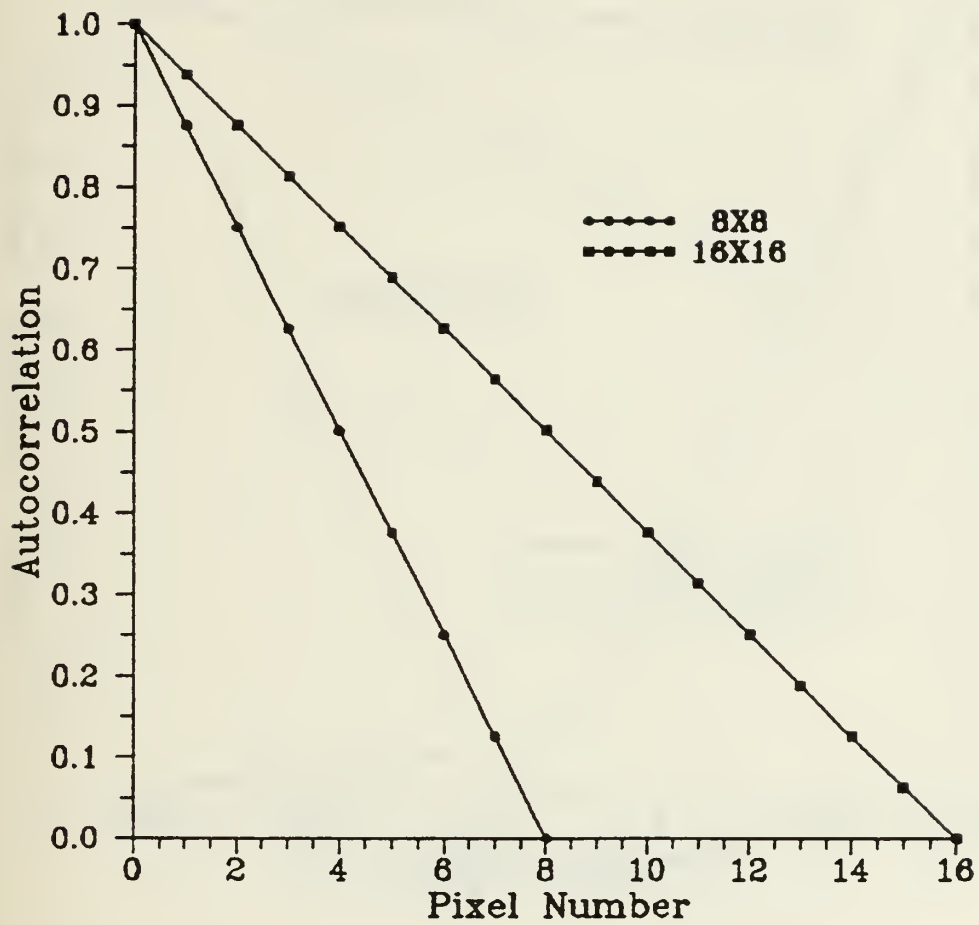


Figure 10. Computed Autocorrelation of a Square Subaperture.

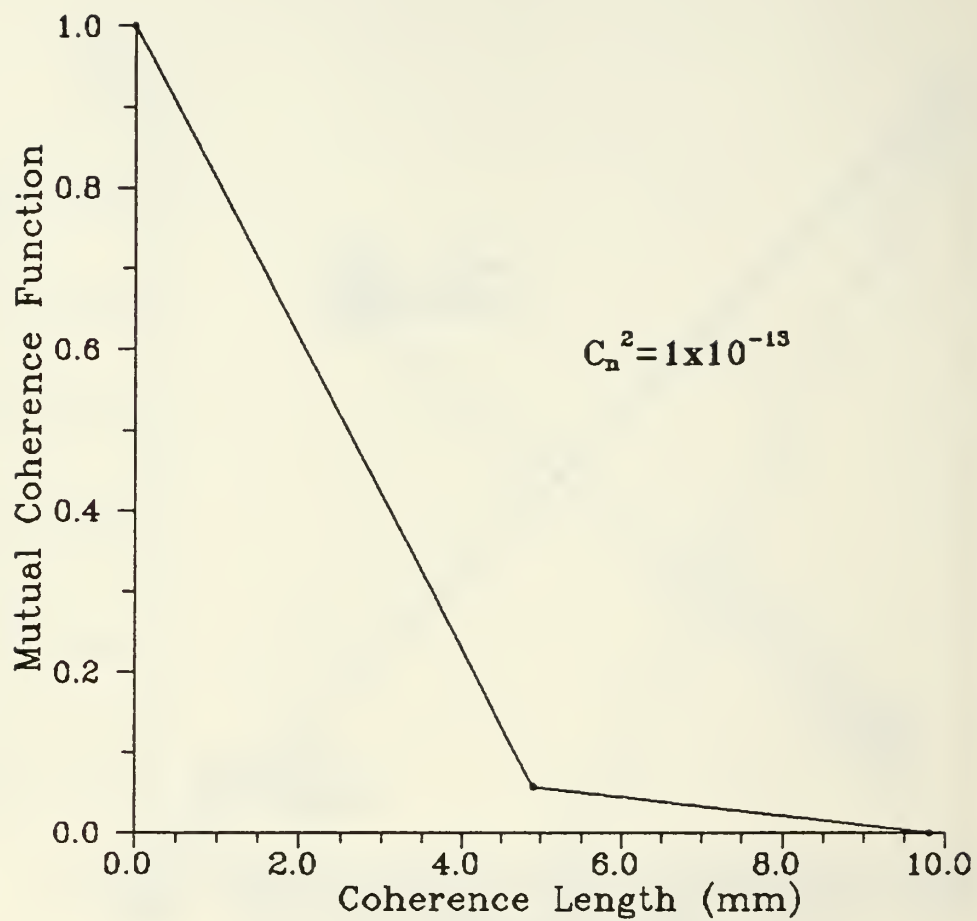


Figure 11. Mutual Coherence Function of a 64 x 64 Subaperture.

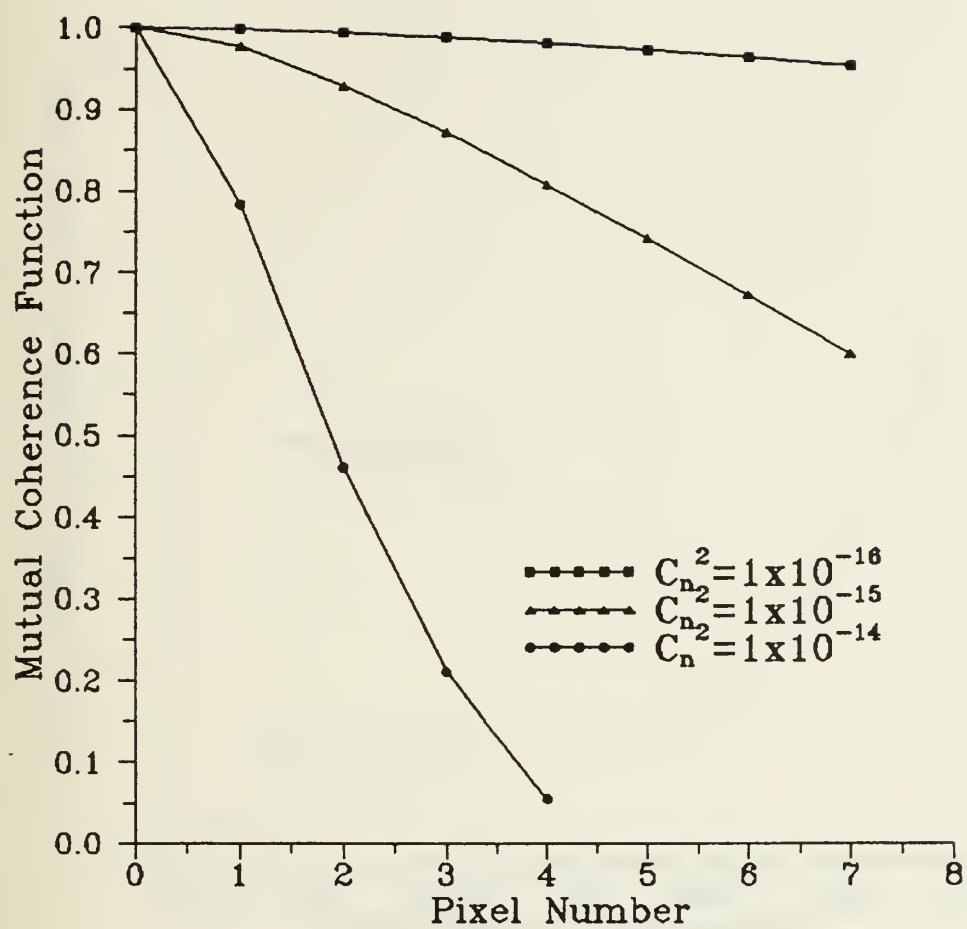


Figure 12. Mutual Coherence Function Trends.

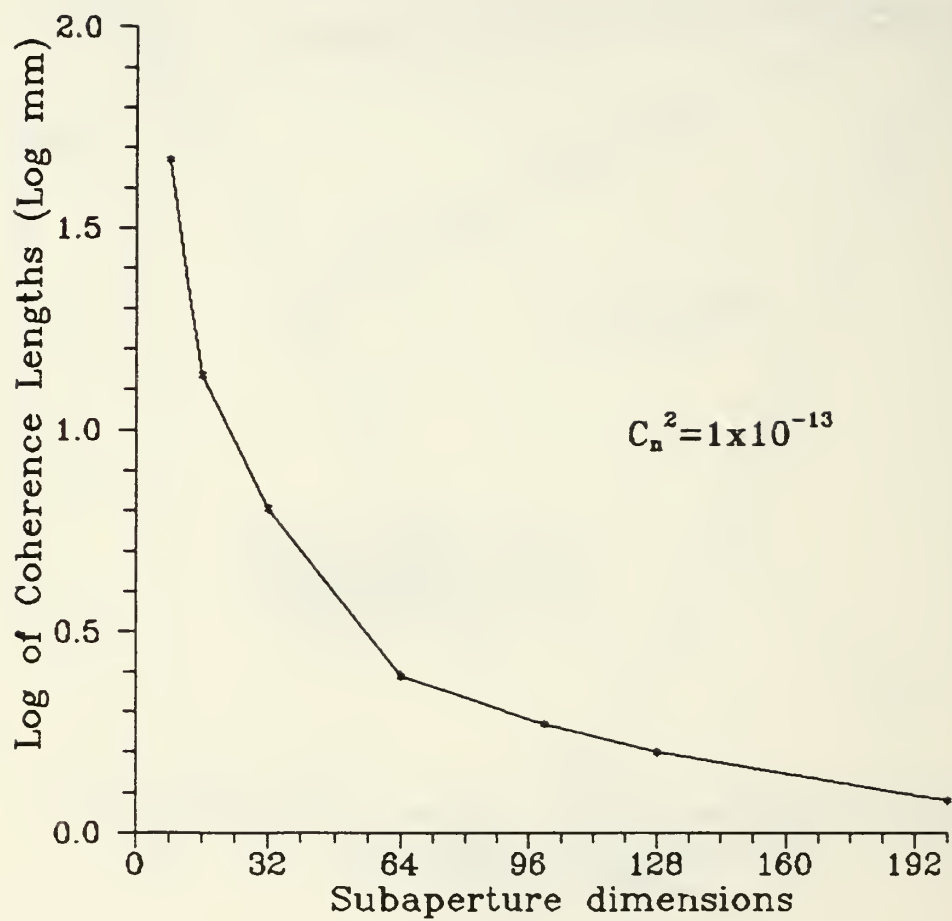


Figure 13. Subaperture Coherence Lengths for  $C_n^2 = 1 \times 10^{-13}$ .

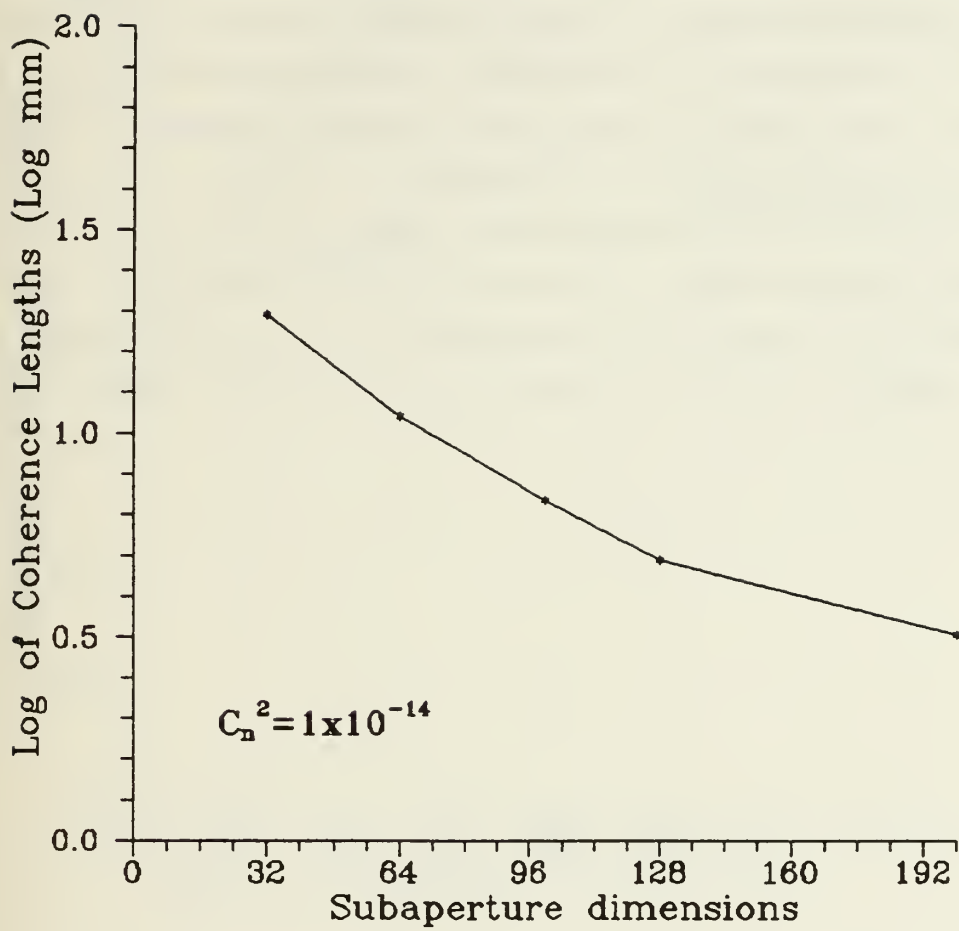


Figure 14. Subaperture Coherence Lengths for  $C_n^2 = 1 \times 10^{-14}$ .

were identical to those for the 256 x 256 dimensioning, within the arithmetic error of the algorithm. The information provided by the 512 dimensioning was that the inaccuracy of the code was not due to an inner scale problem, however, a low frequency, outer scale problem may still exist.

### C. SATURATION

The last area of investigation was whether or not the simulation predicts the saturation of intensity for an extended medium modeled by a single phase screen realization. Saturation is generally considered to be caused by multiple scattering, a scattered wave interfering with a distorted wave. One would expect from the Rytov approximation of turbulence theory, that saturation will occur even in Fraunhofer propagation. This assumption stems from the representation of turbulence in the form,  $e^{\theta}$ , which has a magnitude bounded between plus and minus one. Figure 15 illustrates that the normalized intensity variance saturates with increasing turbulence. Theoretically, a normalized variance of one is expected for Rayleigh statistics. However, it is premature to assume that saturation is inherent in Fraunhofer cases, until the MCF results are verified.

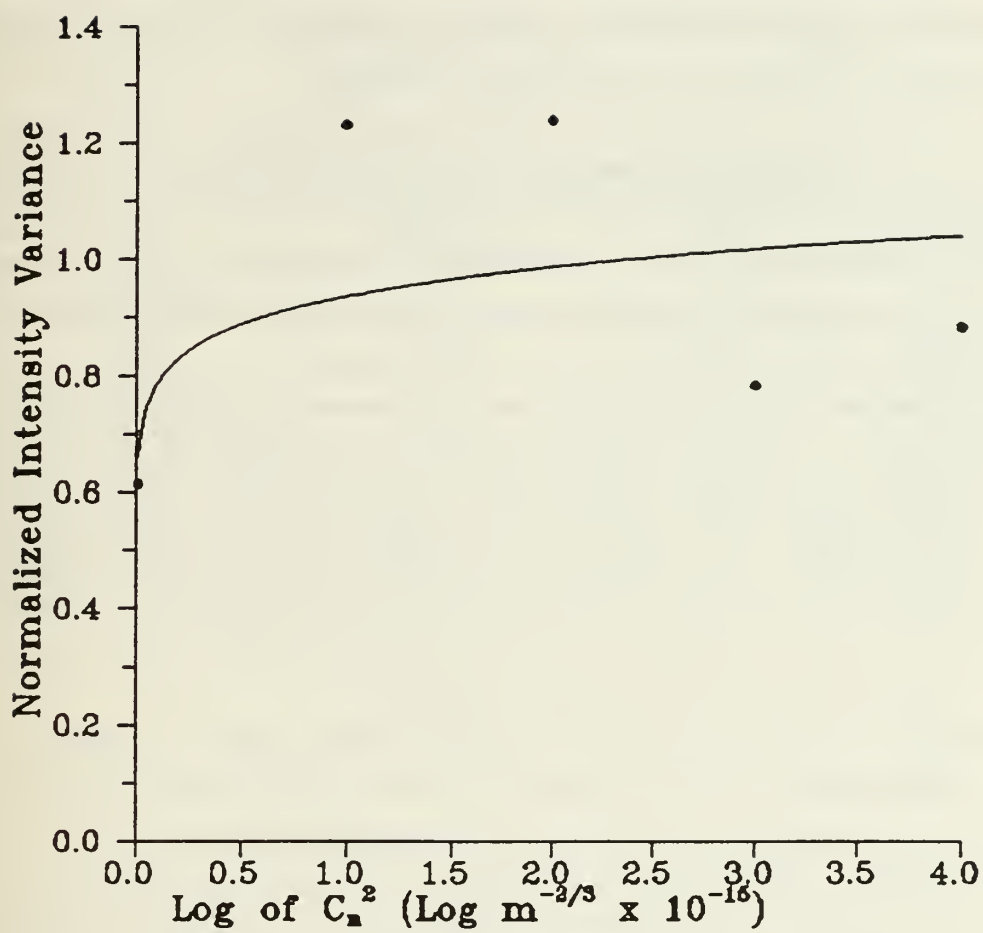


Figure 15. Intensity Variance Saturation of a 16 x 16 Subaperture.

## V. CONCLUSIONS AND RECOMMENDATIONS

This thesis simulated the propagation of plane waves through an extended two-dimensional random media using a single phase screen technique. The atmospheric turbulence had a Kolmogorov  $\kappa^{-11/3}$  pure power law, while the propagation was strictly Fraunhofer. Limitations of its applicability were, primarily, the finite spatial range imposed by the available grid size. Diffraction patterns, correlation functions and intensity variance saturation at the observation plane, were investigated.

The results provided by the simulation suggest general agreement with the turbulence theory. Saturation for weak scattering was supported by this model. The MCF curves, although not completely correct, provided insight to the theory and illustrated problems which are still present in the current coding. Some specific problems include, potential errors in the implementation of the filtering technique from edge effects, aliasing and inner scale problems, or from incorrect normalization.

Any further research on this topic should begin with resolving the inaccuracies still present in the simulation coding. Several possible reasons were presented, however, an error in the filtering of the phase screen seems to be the most likely cause. Further testing can be conducted on the phase screen, to include calculating the phase screen variance, as well as, its structure function  $D_\theta$ . By comparing the simulated phase screen with the theoretical structure function for  $D_\theta$ , this technique will verify whether or not the simulated phase screen accurately represents turbulence.

An assumption was made, that aliasing was not a problem, since the problems associated with undersampling were not apparent. Aliasing can be tested by using finer grid sizes and observing changes induced by the higher spatial frequencies.

After the coding is working correctly, both the convolution and transfer function form of Fresnel propagation can be implemented and exercised. In addition, the array sizes should be modified to incorporate a dimension of 512 or 1024. Finally, during the phase screen generation, *phasei* should be filled with random numbers to give two usable phase screens. It is not obvious whether two independent phase screens will be produced, or whether the total energy will be distributed among the two phase screens. Therefore, testing should be conducted to ensure that each usable phase screen possesses the correct statistics.

## APPENDIX A. RANDOM NUMBER GENERATOR TEST DATA

The following table provides the statistical results of the five empirical tests run on the random number generator,  $Ran(I)$ . The  $X^2$  values were determined from the Chi-Square table in Bevington [Ref 15 ].

The results of the Lagged Product test correspond respectively to the theoretical mean,  $\mu_T$ , calculated mean,  $\mu$ , theoretical standard deviation,  $\sigma_T$ , and calculated standard deviation,  $\sigma$ . A lag of three was tested.

Table 1. RANDOM NUMBER GENERATOR TEST DATA

<i>TEST</i>	<i>DEGREES OF FREEDOM</i>	$X^2$	<i>PROBABILITY</i>	
Frequency	9	4.4	88.3%	
Serial	20	17.1	65.0%	
Up and Down	8	4.1	84.5%	
Above and Below the Mean	12	6.2	90.5%	
<i>TEST</i>	$\mu_T$	$\mu$	$\sigma_T$	$\sigma$
Lagged Product	0.250	0.259	0.100	0.092

## APPENDIX B. FFT TIME SERIES DATA

This appendix contains the results of the comparison between the two FFT sub-routines, *FFT2C* and subroutine *FFT* . A function routine called *SCNDS*, was implemented in the code to provide accurate time measurements.

Table 2. FFT TIME SERIES DATA

<i>COMPUTER SETUP</i>	<i>FFT</i>	<i>FFT2C</i>
1 DIMENSION	TIME(sec)	TIME(sec)
2 <sup>13</sup> with 20-MHz 80387	2.64	2.64
2 <sup>16</sup> with 20-MHz 80387	25.54	25.26
2 <sup>17</sup> with 20-MHz 80387	54.05	53.44
2 DIMENSION	TIME(sec)	TIME(sec)
128 x 128 with 20-MHz 80387	6.86	7.08
256 x 256 with 20-MHz 80387	31.30	32.08
256 x 256 with Weitek	12.08	12.14
256 x 256 with Weitek and common block	11.48	11.56
512 x 512 with Weitek and common block	49.54	52.40

## APPENDIX C. SIMULATION CODE

The simulation code contained in this appendix incorporates Fraunhofer and both forms of Fresnel propagation. This thesis only exercised the Fraunhofer propagation.

```
C *****
C
C THIS CODE PROVIDES A QUALITATIVE VIEW OF BOTH FRAUNHOFER AND
C FRESNEL DIFFRACTION BY OBSERVING THE PERTURBATION IMPOSED ON A
C MONOCHROMATIC PLANE WAVE PROPAGATING THROUGH A TURDULENT
C MEDIUM. THE TURBULENT MEDIUM IS INTRODUCED IN THE FORM OF A
C STOCHASTIC PHASE SCREEN. PROPAGATION OF THE ELECTRIC FIELD IS
C ACCOMPLISHED THROUGH FFT'S.
C
C *****
C
C GLOSSARY OF VARIABLE NAMES:
C
C 1. ARRAYS:
C
C RE - ONE DIMENSION REAL ARRAY OF DIMENSION NR, WHICH IS USED TO
C MANIPULATE THE REAL PART OF THE COMPLEX ELECTRIC FIELD IN
C THE FFT SUBROUTINE. THIS ARRAY IS REPEATEDLY USED THROUGHOUT
C THE CODE.
C
C RIM- ONE DIMENSION REAL ARRAY OF DIMENSION NR, WHICH IS USED
C TO MANIPULATE THE IMAGINARY PART OF THE COMPLEX ELECTRIC
C FIELD IN THE FFT SUBROUTINE. THIS ARRAY IS REPEATEDLY USED
C THROUGHOUT THE CODE.
C
C FIELDR - TWO DIMENSION REAL ARRAY OF DIMENSION NR X NR
C CONTAINING THE REAL PART OF THE COMPLEX ELECTRIC
C FIELD. THIS ARRAY IS REPEATEDLY USED THROUGHOUT THE CODE
C
C FIELDI - TWO DIMENSION REAL ARRAY OF DIMENSION NR X NR
C CONTAINING THE IMAGINARY PART OF THE COMPLEX ELECTRIC
C FIELD. THIS ARRAY IS REPEATEDLY USED THROUGHOUT THE CODE
C
C FILL - TWO DIMENSION REAL ARRAY OF DIMENSION NR X NR USED AS A
C DUMMY ARRAY IN THE IFT OF THE POWER SPECTRUM WHICH YIELDS
C THE MCF.
C
C FIELDM - TWO DIMENSION ARRAY OF DIMENSION NR X NR REPRESENTING
C THE MAGNITUDE OF THE PERTURBED ELECTRIC FIELD.
C
C FMCF - TWO DIMENSION ARRAY OF DIMENSION NR X NR REPRESENTING THE
C INTENSITY OF THE PERTURBED ELECTRIC FIELD. THIS ARRAY IS
C USED IN DETERMINING THE MCF.
C
C FNORM - TWO DIMENSION ARRAY OF DIMENSION NR X NR REPRESENTING THE
```

INTENSITY OF THE UNPERTURBED ELECTRIC FIELD. THIS ARRAY IS ALSO USED IN DETERMINING THE MCF.

PHASER - TWO DIMENSION REAL ARRAY OF DIMENSION NR X NR CONTAINING THE REAL PART OF THE RANDOM COMPLEX PHASE SCREEN.

PHASEI - TWO DIMENSION REAL ARRAY OF DIMENSION NR X NR CONTAINING THE IMAGINARY PART OF THE RANDOM COMPLEX PHASE SCREEN.

FMAG - ONE DIMENSION SLICE OF THE PERTURBED MCF USED IN THE GRAPHICS ROUTINE. REAL ARRAY.

DIST - ONE DIMENSION REAL ARRAY REPRESENTING THE PIXELS CORRESPONDING TO THE VALUES IN THE ARRAY FMAG.

VARIABLES:

NR - DIMENSION OF THE ARRAYS EXACTLY AS SPECIFIED IN THE DIMENSION STATEMENTS IN THE CALLING PROGRAM. INPUT INTEGER. INDICE.

N2 - ONE HALF OF NR. INTEGER.

M - POWER OF 2 IN THE DIMENSIONING. USED IN THE FFT SUBROUTINE.

ISIZE - INTEGER VALUE CORRESPONDING TO A PARTICULAR CHOICE FOR AN APERTURE SIZE. INPUT VARIABLE.

NSIZE - INTEGER VALUE CORRESPONDING TO THE ACTUAL APERTURE SIZE.

DELSH - REAL VALUE REPRESENTING THE SAMPLING INTERVAL FOR A PARTICULAR APERTURE SIZE.

SEED - REAL INPUT VARIABLE USED TO BEGIN A RANDOM SEQUENCE OF NUMBERS FOR THE SUBROUTINE GGAUS.

NYES - INPUT INTEGER VARIABLE WHICH SELECTS WHETHER TURBULENCE IS INTRODUCED IN THE CODE.

FILTER - FIXED INPUT VALUE USED IN THE FILTERING FUNCTION. REAL.

CN2 - REAL INPUT VARIABLE REPRESENTING THE INDEX-OF-REFRACTION STRUCTURE PARAMETER. DETERMINES THE AMOUNT OF TURBULENCE INTRODUCED IN THE FILTERING FUNCTION.

DREC - REAL INPUT VARIABLE REPRESENTING THE RECEIVING FIELD SIZE.

DTRNS - FIXED VALUE FOR THE TRANSMITTING FIELD SIZE. REAL.

Z - REAL INPUT VARIABLE REPRESENTING THE TOTAL PROPAGATION DISTANCE OF THE ELECTRIC FIELD.

DELX - REAL VARIABLE FOR THE PROPAGATION DISTANCE TO EACH SLAB.

NUMSCR - INTEGER INPUT VARIABLE USED IN NEAR-FIELD FRESNEL PROPAGATION. THIS VARIABLE CORRESPONDS THE THE NUMBER OF EQUALLY SPACED SLABS WHICH MAKE UP THE TOTAL DISTANCE.

WVL - FIXED VALUE FOR THE WAVELENGTH.  
 ICNT - INTEGER VALUE WHICH DETERMINES WHETHER OR NOT THE FIELD HAS  
 PROPAGATED THE TOTAL DISTANCE Z. USED IN NEAR-FIELD  
 FRESNEL PROPAGATION.  
 PI - VALUE OF PI.  
 TPI - TWICE THE VALUE OF PI.  
 MODE - REAL VALUE WHICH DETERMINES THE FORM OF PROPAGATION.  
 SIGN - REAL VALUE EITHER 1.0 OR -1.0 WHICH DETERMINES WHETHER THE  
 FFT IS DIRECT OR INDIRECT. IT ALSO DETERMINES WHETHER  
 NORMALIZATION OCCURS.  
 FLDM - MAXIMUM VALUE IN THE PERTURBED MCF ARRAY.  
 FMAX - MAXIMUM VALUE IN THE PERTURBED ELECTRIC FIELD ARRAY.  
 GRAPHICS:  
 THE FOLLOWING VARIABLE NAMES ARE EITHER SPECIFIC TO THE SVS  
 GRAPHICS ROUTINE OR USED TO MANIPULATE DATA FOR GRAPHING:  
 NDEX, IREG, ANS, GETC, IUNITP, IUNITV, ISYMB, ITNO, MON, NPRIN,  
 MODE, ONE, TITLE, IX, IY, XMAX, ICOLOR, INCR, NTOT.

\*\*\*\*\*

```

COMMON /BLK1/ RE(256),RIM(256)
COMMON /BLK2/ FIELDR(256,256),FIELDI(256,256)
COMMON /BLK3/ PHASER(256,256),PHASEI(256,256)
DIMENSION NDEX(20),FLDM(256,256),FMCF(256,256),FNORM(256,256)
DIMENSION FMAG(130),DIST(130),FILL(256,256)
INTEGER*2 IREG(9)
DOUBLE PRECISION PI
DATA NDEX/15,15,7,7,8,8,14,14,5,5,4,4,2,2,3,3,1,1,0,0/
DATA RE/256*0.0/,RIM/256*0.0/
DATA FMAG/130*0.0/,DIST/130*0.0/
CHARACTER*4 ONE
CHARACTER*21 TITLE
CHARACTER*2 ANS,GETC
DATA TITLE/'THE SEED VALUE IS= '/
DATA ONE/' '/
DATA IUNITP/10/,IUNITV/20/
OPEN(4,FILE='LN.DAT',STATUS='NEW')
ISYMB=22
ITNO=5
MON=18
PI=3.141592653589792
NPRIN=0
MODE=0
  
```

999 CONTINUE

C  
C  
C  
C

THIS SECTION OF THE PROGRAM SETS UP THE INPUT PARAMETERS FOR THE  
SIMULATION.

```
WRITE(*,*)'  
WRITE(*,*)'HELLO... LET US BEGIN THIS SIMULATION BY ENTERING '  
WRITE(*,*)'SEVERAL INPUT PARAMETER VALUES.'  
WRITE(*,*)'  
WRITE(*,*)'THE VARIABLE WHICH DIMENSIONS THE ARRAY SIZE IS THE '  
WRITE(*,*)'FIRST VALUE TO ENTER. INPUT THE INTEGER VALUE.'  
READ(*,*)NR  
WRITE(*,*)'  
WRITE(*,*)'THE SECOND VARIABLE OF INTEREST IS "NSIZE". THIS '  
WRITE(*,*)'VARIABLE DIMENSIONS THE SIZE OF THE PLANAR ELECTRIC '  
WRITE(*,*)'FIELD. SELECT ONE OF THE FOLLOWING.'  
WRITE(*,*)'          1. FOR 100 X 100 '  
WRITE(*,*)'          2. FOR 64 X 64 '  
WRITE(*,*)'          3. FOR 32 X 32 '  
WRITE(*,*)'          4. FOR 16 X 16 '  
WRITE(*,*)'          5. FOR 8 X 8 '  
WRITE(*,*)'          6. FOR 4 X 4 '  
WRITE(*,*)'          7. FOR 2 X 2 '  
WRITE(*,*)'  
READ(*,*)ISIZE  
IF(ISIZE.EQ.1) THEN  
    NSIZE=50  
    DELMSH=.0031  
    INCR=3  
ELSEIF(ISIZE.EQ.2) THEN  
    NSIZE=32  
    DELMSH=.0049  
    INCR=1  
ELSEIF(ISIZE.EQ.3) THEN  
    NSIZE=16  
    DELMSH=.0098  
    INCR=2  
ELSEIF(ISIZE.EQ.4) THEN  
    NSIZE=8  
    DELMSH=.019531  
    INCR=2  
ELSEIF(ISIZE.EQ.5) THEN  
    NSIZE=4  
    DELMSH=.039063  
    INCR=1  
ELSEIF(ISIZE.EQ.6) THEN  
    NSIZE=2  
    DELMSH=.0781  
    INCR=1  
ELSE  
    NSIZE=1  
    DELMSH=.1563  
    INCR=1  
ENDIF  
WRITE(*,*)'  
WRITE(*,*)'ANOTHER INPUT PARAMETER IS THE SEED VALUE OF THE'
```

```

WRITE(*,*)'RANDOM NUMBER GENERATOR. INPUT THE SEED VALUE OF +1.0'
WRITE(*,*)'OR -1.0'
READ(*,*)SEED
WRITE(*,*)'
WRITE(*,*)'FINALLY INPUT AN INTEGER OF VALUE 1 FOR TURBULENCE, OR'
WRITE(*,*)'0 FOR NO TURBULENCE.'
READ(*,*)NYES
IF(NYES.EQ.1) THEN
WRITE(*,*)'
WRITE(*,*)'INPUT THE VALUE OF FILTER'
READ(*,*)FILTER
ENDIF
WRITE(*,*)'
WRITE(*,*)'INPUT THE VALUE FOR CN2'
READ(*,*)CN2
WRITE(*,*)'
c WRITE(*,*)'INPUT THE RECEIVING FIELD SIZE IN METERS'
c READ(*,*)DREC
WRITE(*,*)'
WRITE(*,*)'INPUT THE TOTAL PROPAGATION DISTANCE IN METERS'
READ(*,*)Z
WRITE(*,*)'
c WRITE(*,*)'INPUT THE NUMBER OF SCREENS TO BE USED EITHER FOR'
c WRITE(*,*)'FRESNEL OR FRAUNHOFER '
c READ(*,*)NUMSCR
IF(SEED.GE.1.0) THEN
ONE(1:2)='+1'
ELSE
ONE(1:2)='-1'
ENDIF
TITLE(20:21)=ONE(1:2)
N2=NR/2
WVL=.5E-6
M=ALOG(REAL(NR))/ALOG(2.)
DTRNS=.3125
ICNT=0

C
C THE FOLLOWING STATEMENT DETERMINES WHICH FORM OF FRESNEL IS TO BE
C USED
C
c MODE=INT((2*DTRNS*DREC)/(WVL*Z))
C
C THE FOLLOWING SUBROUTINE CALLED MCF DETERMINES THE AUTOCORRELATION
C OF THE APERTURE WHICH IS TO BE USED IN DETERMINING THE ATMOSPHERIC
C COHERENCE LENGTH.
C
CALL MCF(FNORM,NR,M,PI,NSIZE,N2,DELSH)
C
C THIS SECTION CREATES THE PLANAR ELECTRIC FIELD
C
DO 40 I=1,NR
DO 40 J=1,NR
FIELDR(I,J)=0.0
FIELDI(I,J)=0.0
40 CONTINUE
DO 41 I=N2-NSIZE+1,N2+NSIZE

```

```

      DO 41 J=N2-NSIZE+1,N2+NSIZE
        FIELDR(I,J)=1.0
41 CONTINUE
C
C   THIS SECTION DETERMINES THE SLAB THICKNESS(ES) FOR WHICH THE
C   ELECTRIC FIELD IS PROPAGATED THROUGH.THIS IS VALID FOR BOTH
C   FORMS OF PROPAGATION.
C
C   IF(NR.LE.MODE) THEN
C     DELX=Z/NUMSCR
C   ELSE
C     DELX=Z
C
C   THE FOLLOWING SUBROUTINE PLACES A CURVATURE ON THE WAVEFRONT TO BE
C   USED FOR THE CONVOLUTION FORM OF FRESNEL PROPAGATION.
C
C   CALL QUAD1(NR,PI,DELSH,DX,DY,WVL,DELX)
C   ENDIF
C
1000 CONTINUE
C
C   THIS SECTION CALLS OUT GAUSSIAN RANDOM NUMBERS FOR THE REAL AND
C   IMAGINARY PHASE ARRAYS.
C
C   CALL GGAUS(NR,SEED)
C
C   THIS BEGINS THE FILTERING PROCESS OF THE PHASE SCREEN
C
C   CALL FLTR(NR,DELSH,CN2,DELX,WVL,FILTER)
C
C   HERE THE INDIRECT TRANSFORM IS BEING APPLIED TO THE FILTERED
C   PHASE SCREENS.
C
C   CALL IFTSCR(NR,M,DELSH)
C
C   THE FOLLOWING ARRAYS USED IN THE FFT ROUTINES ARE ZEROED OUT TO
C   ENSURE THAT UNWANTED VALUES ARE NOT LEFT IN THE ARRAYS.
C
      DO 990 I=1,NR
        RE(I)=0.0
        RIM(I)=0.0
990 CONTINUE
C
C   THIS SECTION DOES THE ALGEBRA NEEDED TO MESH THE PHASE SCREEN
C   TOGETHER WITH THE ELECTRIC FIELD
C
      DO 50 I=1,NR
        DO 50 J=1,NR
          XA=COS(PHASER(I,J))*FIELDR(I,J)
          XB=COS(PHASER(I,J))*FIELDI(I,J)
          XC=SIN(PHASER(I,J))*FIELDR(I,J)
          XD=SIN(PHASER(I,J))*FIELDI(I,J)
          FIELDR(I,J)=XA-XD
          FIELDI(I,J)=XB+XC
50 CONTINUE
C

```

```

C      HERE THE FAST FOURIER TRANSFORM IS BEING APPLIED TO THE PERTURBED
C      ELECTRIC FIELD. FOR A DIRECT TRANSFORM SIGN=-1.0, AND INDIRECT
C      TRANSFORM SIGN=+1.0.
C
C      SIGN=-1.0
C      CALL DFTIFT(NR,M,SIGN,DELMISH)
C
C      DO 141 I=1,NR
C        DO 141 J=1,NR
C          FIELDR(I,J)=FIELDR(I,J)/(NR*DELMISH)
C          FIELDI(I,J)=FIELDI(I,J)/(NR*DELMISH)
141  CONTINUE
C
C
C      THIS PORTION OF THE IF STATEMENT CORRESPONDS TO THE IMPLEMENTATION
C      OF THE TRANSFER FUNCTION FORM OF FRESNEL PROPAGATION. THE
C      SUBROUTINE CALLED TRNSFR APPLIES A QUADRATIC TO THE FIELD.
C
C      IF(NR.LE.MODE) THEN
C        CALL TRNSFR(NR,PI,DX,DY,WVL,DELX,DTRNS)
C        ICNT=ICNT+1
C        SIGN=+1.0
C        CALL DFTIFT(NR,M,SIGN,DELMISH)
C        GO TO 888
C      ELSE
C
C        THE SUBROUTINE CALLED QUAD2 PUTS THE DIFFRACTION PATTERN IN REAL
C        SPACE COORDINATES.
C
C        CALL QUAD2(NR,PI,DX,DY,WVL,DELX)
C      ENDIF
C
C 888  CONTINUE
C
C
C      THIS DO LOOP DETERMINES THE POWER SPECTRAL DENSITY AND SETS IT UP
C      FOR AN FFT TO DETERMINE THE MCF.
C
C      DO 152 I=1,NR
C        DO 152 J=1,NR
C          FMC(I,J)=FIELDR(I,J)**2+FIELDI(I,J)**2
C          FILL(I,J)=0.0
152  CONTINUE
C
C      ONCE AGAIN THE ARRAYS ARE CLEARED OF STRAY VALUES
C
C      DO 910 I=1,NR
C        RE(I)=0.0
C        RIM(I)=0.0
910  CONTINUE
C
C      THE INVERSE FFT IS APPLIED TO THE POWER SPECTRAL DENSITY
C
C      SIGN=+1.0
C      DO 901 I=1,NR
C        DO 911 J=1,NR

```

```

        RE(J)=FMCF(I,J)
        RIM(J)=FILL(I,J)
911 CONTINUE
        CALL FFT(M,SIGN,DELMISH)
        DO 921 J=1,NR
            FMCF(I,J)=RE(J)
            FILL(I,J)=RIM(J)
921 CONTINUE
901 CONTINUE
        DO 931 J=1,NR
            DO 941 I=1,NR
                RE(I)=FMCF(I,J)
                RIM(I)=FILL(I,J)
941 CONTINUE
        CALL FFT(M,SIGN,DELMISH)
        DO 951 I=1,NR
            FMCF(I,J)=RE(I)
            FILL(I,J)=RIM(I)
951 CONTINUE
931 CONTINUE
C
C
C   THIS SECTION DETERMINES THE MAXIMUM VALUE AND NORMALIZES THE MCF
C
        FLDM=0.0
        DO 89 I=1,NR
            DO 89 J=1,NR
                XMG=FMCF(I,J)
                IF(XMG.GT.FLDM) THEN
                    FLDM=XMG
                ENDIF
89 CONTINUE
C   WRITE(*,*) FLDM
C   PAUSE
C
C   THE MCF IS NORMALIZED SO THE MAX VALUE IS 1.0
C
        DO 29 I=1,N2
            DO 29 J=1,N2
                FMCF(I,J)=FMCF(I,J)/FLDM
29 CONTINUE
C
C   THE ATMOSPHERIC MCF IS DETERMINED BY DIVIDING OUT THE APERTURE
C   FUNCTION FROM THE PERTURBED ELECTRIC FIELD MCF.
C
        DO 91 I=1,N2
            DO 91 J=1,N2
                FMCF(I,J)=FMCF(I,J)/FNORM(I,J)
91 CONTINUE
C
C
C   DO 87 I=1,1
C       DO 87 J=1,20
C           WRITE(*,*)FMCF(I,J)
C   87 CONTINUE

```

```

C      PAUSE
C
C      THIS SECTION SETS UP THE ARRAYS TO PLOT THE 2-D MCF
C
C      NTOT=2*NSIZE
C      DO 827 I=1,1
C          DO 827 J=1,NTOT
C              DIST(J)=J
C              FMAG(J)=FMCF(I,J)
C      827 CONTINUE
C
C      DO 83 J=1,NTOT
C          WRITE(*,*)FMAG(J),DIST(J)
C      83 CONTINUE
C      PAUSE
C
C      THE FOLLOWING SUBROUTINES ARE FOR THE GRAPHICS PACKAGE
C      THE ATMOSPHERIC MCF IS BEING PLOTTED AT THIS POINT
C
C      CALL VSINIT(18,8.,10.,0,'MCF1.PLT',IUNITV,IVID,5)
C      CALL ORIGIN(.5,1.5,0)
C      CALL SCALE(FMAG,5.,NTOT,1)
C      CALL AXIS(0.,0.,'MCF',0,1,1,5.,90.,FMAG(NTOT+1),FMAG(NTOT+2),.1,1)
C      CALL SCALE(DIST,5.,NTOT,1)
C      CALL AXIS(0.,0.,'I',0,-1,-1,5.,0.,DIST(NTOT+1),DIST(NTOT+2),.1,1)
C      CALL LINES(DIST,FMAG,NTOT,1,-1,ISYMB,.1)
C      CLOSE(IUNITV)
C      CALL INT86(ITNO,IREG)
C      CALL MSG(0.,0.,.15,'PRESS ANY KEY TO CONTINUE',0.,0,1)
C      ANS=GETC()
C      CALL GMODE(IVID)
C
C
C      THE MAGNITUDE OF THE FFT'D ELECTRIC FIELD IS CALCULATED IN ORDER
C      TO PLOT THE OUTPUT.
C
C
C      FMAX=0.0
C      DO 80 I=1,NR
C          DO 80 J=1,NR
C              FIELDM(I,J)=SQRT(FIELDI(I,J)**2+FIELDI(I,J)**2)
C              X=FIELDM(I,J)
C              IF(X.GT.FMAX) THEN
C                  FMAX=X
C              ENDIF
C      80 CONTINUE
C
C      THIS SECTION BEGINS THE CALLING SEQUENCE FOR PLOTTING
C
C      CALL VSINIT(MON,10.,8.,0,'DITHER.PLT',IUNITV,IVID,5)
C      DO 100 I=1,N2
C          DO 100 J=1,N2
C              IX=J*INCR
C              IY=I*INCR
C              XMAX=ALOG10(FIELDM(I,J)/FMAX)

```

```

        INDEX=8*ABS(XMAX)+1
        IF(INDEX.GE.21) THEN
            ICOLOR=0
        ELSE
            ICOLOR=NDEX(INDEX)
        ENDIF
        CALL PIXEL(IX,IY,ICOLOR)
100 CONTINUE
        CALL MSG(0.,1.,.15,TITLE,0.,0,0)
        CLOSE(IUNITV)
C       CALL INT86(1TNO,IREG)
        CALL MSG(0.,0.,.15,'PRESS ANY KEY TO CONTINUE',0.,0,0)
        ANS=GETC()
        CALL GMODE(IVID)
C
C       THIS IF STATEMENT QUES THE PROGRAM TO START OVER AGAIN IF
C       FRAUNHOFER OR THE CONVOLUTION FORM OF FRESNEL ARE USED
C
        IF(NR.GT.MODE) THEN
            GO TO 999
        ENDIF
C
C       THIS IF STATEMENT QUES THE PROGRAM TO FULLY COMPLETE PROPAGATION
C       THROUGH ALL THE SLABS IN THE TRANSFER FUNCTION FORM OF FRESNEL
C
        IF(ICNT.NE.NUMSCR) THEN
            GO TO 1000
        ENDIF
        GO TO 999
    END
C
    SUBROUTINE QUAD1(NR,PI,DELMISH,DX,DY,WVL,DELX)
    COMMON /BLK2/ FIELDR(256,256),FIELDI(256,256)
    DX=DELMISH
    DY=DELMISH
    MID=(NR/2)+1
    DO 273 I=1,NR
        X=(I-(MID*2-1))*DX
        DO 273 J=1,NR
            Y=(J-(MID*2-1))*DY
            THETA=PI*(((X*X)+(Y*Y))/(WVL*DELX))
            XX=FIELDR(I,J)*COS(THETA)
            YY=FIELDR(I,J)*SIN(THETA)
            ZZ=FIELDI(I,J)*COS(THETA)
            WW=FIELDI(I,J)*SIN(THETA)
            FIELDR(I,J)=XX-WW
            FIELDI(I,J)=YY+ZZ
273 CONTINUE
        RETURN
    END
C
    SUBROUTINE QUAD2(NR,PI,DX,DY,WVL,DELX)
    COMMON /BLK2/ FIELDR(256,256),FIELDI(256,256)
    DX2=DX*WVL*DELX
    DY2=DY*WVL*DELX
    MID=NR/2+1

```

```

DO 274 I=1,NR
  Y=(I-MID)*DY2
DO 274 J=1,NR
  X=(J-MID)*DX2
  PHI=PI*((X*X)+(Y*Y))/(WVL*DELX))
  CX=FIELDR(I,J)*COS(PHI)
  CY=FIELDR(I,J)*SIN(PHI)
  CZ=FIELDI(I,J)*COS(PHI)
  CW=FIELDI(I,J)*SIN(PHI)
  CBR=CX-CW
  CBI=CY+CZ
  FIELDR(I,J)=(CBI/(WVL*DELX))
  FIELDI(I,J)=-1.*(CBR/(WVL*DELX))

```

```

274 CONTINUE
RETURN
END

```

C

```

SUBROUTINE TRNSFR(NR,PI,DX,DY,WVL,DELX,DTRNS)
COMMON /BLK2/ FIELDR(256,256),FIELDI(256,256)
DX=DTRNS/NR
DY=DTRNS/NR
MID=NR/2+1
DO 275 I=1,NR
  FY=(I-MID)*DY
DO 275 J=1,NR
  FX=(J-MID)*DX
  FEE=-1.*PI*WVL*DELX*((FX*FX)+(FY*FY))
  GX=FIELDR(I,J)*COS(FEE)
  GY=FIELDR(I,J)*SIN(FEE)
  GZ=FIELDI(I,J)*COS(FEE)
  GW=FIELDI(I,J)*SIN(FEE)
  FIELDR(I,J)=GX-GW
  FIELDI(I,J)=GY+GZ

```

```

275 CONTINUE
RETURN
END

```

C  
C  
C

```

SUBROUTINE FLTR(NR,DELMISH,CN2,DELX,WVL,FILTER)
NOTE: DELMISH*NR IS THE LARGEST APERTURE SIZE
COMMON /BLK3/ PHASER(256,256),PHASEI(256,256)
PI=3.141592653589792
POWER=-11./6.
TPI=2.*PI
N2=NR/2
NPIVOT=N2+1
LAST=NPIVOT+1
DLKAPA=(TPI/(NR*DELMISH))**POWER
FACTOR=SQRT((TPI**3)*.033*CN2*DELX/(WVL**2))
FUDGE=DLKAPA*FACTOR
DO 100 I=1,NPIVOT
  EYE=REAL(I)
  EYE2=EYE*EYE
DO 100 J=1,NR
  IF(J.LE.NPIVOT) THEN

```

```

        WHY=REAL(J)
        ELSE
        WHY=REAL(NR-J+2)
    ENDIF
    XKAPPA=SQRT(EYE2+WHY*WHY)
    AKAPPA=XKAPPA**FILTER
    PHASER(I,J)=PHASER(I,J)*FUDGE*AKAPPA
    PHASEI(I,J)=PHASEI(I,J)*FUDGE*AKAPPA
100 CONTINUE
    DO 110 I=LAST, NR
        EYE=REAL(NR-I+2)
        EYE2=EYE*EYE
        DO 110 J=1, NR
            IF(J.LE.NPIVOT) THEN
                WHY=REAL(J)
                ELSE
                WHY=REAL(NR-J+2)
            ENDIF
            XKAPPA=SQRT(EYE2+WHY*WHY)
            AKAPPA=XKAPPA**FILTER
            PHASER(I,J)=PHASER(I,J)*FUDGE*AKAPPA
            PHASEI(I,J)=PHASEI(I,J)*FUDGE*AKAPPA
110 CONTINUE
C
    PHASER(1,1)=0.0
    PHASEI(1,1)=0.0
C
C
NOTE: .03441=TPI**-11./6. TO TRANSFORM FROM KAPPA TO FREQ SPACE.
DO 11 I=1, NR
    DO 11 J=1, NR
        PHASER(I,J)=PHASER(I,J)*.03441
        PHASEI(I,J)=PHASEI(I,J)*.03441
11 CONTINUE
RETURN
END
C
SUBROUTINE IFTSCR(NR,M,DELMISH)
COMMON /BLK1/ RE(256),RIM(256)
COMMON /BLK3/ PHASER(256,256),PHASEI(256,256)
PI=3.141592653589792
TPI=2.*PI
SIGN=-1.0
DO 20 I=1, NR
    DO 21 J=1, NR
        RE(J)=PHASER(I,J)
        RIM(J)=PHASEI(I,J)
21 CONTINUE
CALL FFT(M,SIGN,DELMISH)
DO 22 J=1, NR
    PHASER(I,J)=RE(J)
    PHASEI(I,J)=RIM(J)
22 CONTINUE
20 CONTINUE
DO 30 J=1, NR
    DO 31 I=1, NR
        RE(I)=PHASER(I,J)

```

```

        RIM(I)=PHASEI(I,J)
31 CONTINUE
    CALL FFT(M,SIGN,DELMISH)
    DO 32 I=1,NR
        PHASER(I,J)=RE(I)
        PHASEI(I,J)=RIM(I)
32 CONTINUE
30 CONTINUE
    RETURN
    END

```

C

```

SUBROUTINE DFTIFT(NR,M,SIGN,DELMISH)
COMMON /BLK1/ RE(256),RIM(256)
COMMON /BLK2/ FIELDR(256,256),FIELDI(256,256)
DO 60 I=1,NR
    DO 61 J=1,NR
        RE(J)=FIELDR(I,J)
        RIM(J)=FIELDI(I,J)
61 CONTINUE
    CALL FFT(M,SIGN,DELMISH)
    DO 62 J=1,NR
        FIELDR(I,J)=RE(J)
        FIELDI(I,J)=RIM(J)
62 CONTINUE
60 CONTINUE
    DO 70 J=1,NR
        DO 71 I=1,NR
            RE(I)=FIELDR(I,J)
            RIM(I)=FIELDI(I,J)
71 CONTINUE
    CALL FFT(M,SIGN,DELMISH)
    DO 72 I=1,NR
        FIELDR(I,J)=RE(I)
        FIELDI(I,J)=RIM(I)
72 CONTINUE
70 CONTINUE
    RETURN
    END

```

C

C

```

SUBROUTINE FFT(M,SIGN,DELMISH)
COMMON /BLK1/ RE(256),RIM(256)
PI=3.141592653589792*SIGN
N=2**M
N1=N-1
J=1
DO 200 I=1,N1
    IF(I.LT.J) THEN
        T=RE(J)
        RE(J)=RE(I)
        RE(I)=T
        T=RIM(J)
        RIM(J)=RIM(I)
        RIM(I)=T
    END IF
    K=N/2

```

```

DO 201 WHILE(K.LT.J)
    J=J-K
    K=K/2
201 CONTINUE
    J=J+K
200 CONTINUE
    LE=1
    DO 202 L=1,M
        LE1=LE
        LE=LE+LE
        URE=1.
        UIM=0.
        ANG=PI/LE1
        WRE=COS(ANG)
        WIM=SIN(ANG)
    DO 203 J=1,LE1
        DO 204 I=J,N,LE
            IP=I+LE1
            TRE=RE(IP)*URE-RIM(IP)*UIM
            TIM=RE(IP)*UIM+RIM(IP)*URE
            RE(IP)=RE(I)-TRE
            RIM(IP)=RIM(I)-TIM
            RE(I)=RE(I)+TRE
            RIM(I)=RIM(I)+TIM
204 CONTINUE
            T=URE*WRE-UIM*WIM
            UIM=URE*WIM+UIM*WRE
            URE=T
203 CONTINUE
202 CONTINUE
        IF(SIGN.GT.0.0) THEN
            PTS=1.0/(N*DELMISH)
            DO 205 I=1,N
                RE(I)=RE(I)*PTS
                RIM(I)=RIM(I)*PTS
205 CONTINUE
            ENDIF
            RETURN
        END
C
C
SUBROUTINE GGAUS(NR,SEED)
COMMON /BLK3/ PHASER(256,256),PHASEI(256,256)
DO 300 I=1,NR
    DO 300 J=1,NR
301 V1=2.*RAN(SEED)-1
    V2=2.*RAN(SEED)-1
    S=V1*V1+V2*V2
    IF(S.GE.1.0) GO TO 301
    SCALE=SQRT(-2.*ALOG(S)/S)
    X1=V1*SCALE
    X2=V2*SCALE
C
    PHASER(I,J)=X1
    PHASEI(I,J)=0.0
300 CONTINUE
    RETURN

```

```

END
C
SUBROUTINE MCF(FNORM,NR,M,PI,NSIZE,N2,DELMISH)
COMMON /BLK1/ RE(256),RIM(256)
COMMON /BLK2/ FIELDR(256,256),FIELDI(256,256)
DIMENSION FNORM(256,256)
C
C THIS SECTION CREATES THE PLANAR ELECTRIC FIELD
C
DO 39 I=1,NR
  DO 39 J=1,NR
    FIELDR(I,J)=0.0
    FIELDI(I,J)=0.0
39 CONTINUE
C
DO 45 I=N2-NSIZE+1,N2+NSIZE
  DO 45 J=N2-NSIZE+1,N2+NSIZE
    FIELDR(I,J)=1.0
45 CONTINUE
C
C SIGN=-1.0
CALL DFTIFT(NR,M,SIGN,DELMISH)
C
C DO 80 I=1,NR
  DO 80 J=1,NR
    FNORM(I,J)=FIELDR(I,J)**2+FIELDI(I,J)**2
80 CONTINUE
C
DO 123 I=1,NR
  DO 123 J=1,NR
    FIELDI(I,J)=0.0
123 CONTINUE
C
SIGN=+1.0
DO 90 I=1,NR
  DO 91 J=1,NR
    RE(J)=FNORM(I,J)
    RIM(J)=FIELDI(I,J)
91 CONTINUE
CALL FFT(M,SIGN,DELMISH)
DO 92 J=1,NR
  FNORM(I,J)=RE(J)
  FIELDI(I,J)=RIM(J)
92 CONTINUE
90 CONTINUE
DO 93 J=1,NR
  DO 94 I=1,NR
    RE(I)=FNORM(I,J)
    RIM(I)=FIELDI(I,J)
94 CONTINUE
CALL FFT(M,SIGN,DELMISH)
DO 95 I=1,NR
  FNORM(I,J)=RE(I)
  FIELDI(I,J)=RIM(I)

```

```

95 CONTINUE
93 CONTINUE
C
C
  FLDM=0.0
  DO 88 I=1,NR
    DO 88 J=1,NR
      XMG=FNORM(I,J)
      IF(XMG.GT.FLDM) THEN
        FLDM=XMG
      ENDIF
88 CONTINUE
  DO 89 I=1,N2
    DO 89 J=1,N2
      FNORM(I,J)=FNORM(I,J)/FLDM
89 CONTINUE
C
  RETURN
  END

```

## LIST OF REFERENCES

1. Walters, D. L., "Propagation through Atmospheric Turbulence," *High Energy Laser Propagation Handbook*, Chapter 5, Optimetrics, Inc., Ann Arbor, Michigan, 1983.
2. Tatarski, V. I., *Wave Propagation in a Turbulent Medium*, Dover Publications, New York, p. 1967,1961.
3. Clifford, S. F., "The Classical Theory of Wave Propagation in a Turbulent Medium," *Topics in Applied Physics, Laser Beam Propagation in the Atmosphere*, v. 25, Chapter 2, Springer-Verlag, 1978.
4. Strohbehn, J. W., "Modern Theories in the Propagation of Optical Waves in a Turbulent Medium," *Topics in Atmosphere*, v. 25, Chapter 3, Springer-Verlag, 1978.
5. Lutomirski, R. F. and Yura, H. T., "Propagation of a Finite Optical Beam in an Inhomogeneous Medium," *Applied Optics*, v. 10, No. 7, p. 1656, July 1971.
6. Hecht, E. and Zajac, A., *Optics*, Chapter 10, Addison-Wesley, Reading, Massachusetts, 1979.
7. Martin, J. M., and Flatte, S. M., "Intensity Images and Statistics for Numerical Simulation of Wave Propagation in 3-D Random Media," *Applied Optics*, v. 27, No. 11, pp. 2111-2126, 1988.
8. Fried, D. L., "Optical Resolution through a Randomly Inhomogeneous Medium for Very Long and Very Short Exposures," *Journal of the Optical Society of America*, v. 56, No. 10, pp.1372-1379, October 1966.
9. The Optical Science Company Report TR-760, *A Wave Optics Propagation Algorithm*, by P. H. Roberts, pp. 1-15, December 1986.

10. Knuth, D. E., *Seminumerical Algorithms: The Art of Computer Programming* , v. 2, Chapter 3, Addison-Wesley, Reading, Massachusetts, 1981.
11. Buckley, R., "Diffraction by a Random Phase-Changing Screen: A Numerical Experiment." *Journal of Atmospheric and Terrestrial Physics* , v. 37, pp. 1431-1446, 10 March 1975.
12. The Optical Science Company Report TR-663, *Phase Screen Generation* , by G. Cochran. p. 2, September 1985.
13. Brigham, O. E., *The Fast Fourier Transform* , pp. 166-169, Prentice-Hall, Inc., Englewood Cliffs, New Jersey, 1974.
14. The Optical Science Company Report TR-45, *A Wave Optics Propagation Algorithm*, by G. A. Tyler and D. L. Fried, pp. 1-43, 1982.
15. Bevington, P. R., *Data Reduction and Error Analysis for the Physical Sciences*. pp. 314-315, McGraw-Hill Book Company, New York, 1969.

## INITIAL DISTRIBUTION LIST

		No. Copies
1.	Defense Technical Information Center Cameron Station Alexandria, VA 22304-6145	2
2.	Library, Code 0142 Naval Postgraduate School Monterey, CA 93943-5002	2
3.	Professor Donald L. Walters, Code 61We Naval Postgraduate School Monterey, CA 93943-5000	5
4.	Mr. Ken J. Johnston, Code 4130 Naval Research Laboratory Washington, D.C. 20375-5000	1
5.	Mr. Bobby Junker, Code 112 Chief of Naval Research 800 N. Quincy Street Arlington, VA 22217	1
6.	Prof. Karlheinz E. Woehler, Code 61Wh Chairman, Department of Physics Naval Postgraduate School Monterey, CA 93943-5004	1
7.	Commanding Officer Surface Warfare Officers School Command Newport, RI 02841 ATTN: LT. R. A. Dumas	1
8.	Gail Tirrell Vaucher, Code 61 Department of Physics Naval Postgraduate School Monterey, CA 93943-5000	1
9.	Commanding Officer Superintendent of Shipbuilding Seattle, WA 98115-5003 ATTN: LT. E. A. Ugorcak	2











Thesis  
U145  
c.1

Ugorcak  
Numerical simulation  
of optical turbulence  
utilizing two-dimensional  
Gaussian phase screens. 1

Thesis  
U145  
c.1

Ugorcak  
Numerical simulation  
of optical turbulence  
utilizing two-dimensional  
Gaussian phase screens.



thesU145

Numerical simulation of optical turbulen



3 2768 000 81957 7

DUDLEY KNOX LIBRARY